FR-PHENO-2011-004
SFB/CPP-11-07
TTK-11-05
TTP11-04

Electroweak corrections to dilepton + jet production at hadron colliders

Ansgar Denner[1], Stefan Dittmaier[2], Tobias Kasprzik[3], Alexander Mück[4]

[1] *Universität Würzburg, Institut für Theoretische Physik und Astrophysik, D-97074 Würzburg, Germany*

[2] *Albert-Ludwigs-Universität Freiburg, Physikalisches Institut, D-79104 Freiburg, Germany*

[3] *Karlsruhe Institute of Technology (KIT), Institut für Theoretische Teilchenphysik, D-76128 Karlsruhe, Germany*

[4] *RWTH Aachen University, Institut für Theoretische Teilchenphysik und Kosmologie, D-52056 Aachen, Germany*

Abstract:
The first calculation of the next-to-leading-order electroweak corrections to Z-boson + jet hadroproduction including leptonic Z-boson decays is presented, i.e. to the production of a charged lepton–anti-lepton final state in association with one hard jet at the LHC and the Tevatron. The Z-boson resonance is treated consistently using the complex-mass scheme, and all off-shell effects as well as the contributions of the intermediate photon are taken into account. The corresponding next-to-leading-order QCD corrections have also been recalculated. The full calculation is implemented in a flexible Monte Carlo code. Numerical results for cross sections and distributions of this Standard Model benchmark process are presented for the Tevatron and the LHC.

March 2011

1 Introduction

The Drell–Yan process is a cornerstone of electroweak (EW) physics at hadron colliders like the Tevatron and the LHC. The production of W and Z bosons (or off-shell photons) with subsequent leptonic decays has both clean signatures and large cross sections. It can potentially be used to measure the luminosity of the collider, to constrain the PDFs, or to calibrate the detector. On the theoretical side, it is a perfect testing ground for our understanding of hadron-collider physics. Combining experimental accuracy and theoretical predictivity allows for a number of precision measurements in spite of the hadron-collider environment. (See e.g. Refs. [1, 2] and references therein.)

At hadron colliders, the EW gauge bosons are almost always produced together with additional QCD radiation. In this work, we focus on the neutral-current Drell–Yan process in which the dilepton pair is produced in association with a hard, visible jet, i.e.

$$\mathrm{pp}/\mathrm{p\bar{p}} \to \mathrm{Z}/\gamma^* + \mathrm{jet} \to l^+l^- + \mathrm{jet} + X. \tag{1.1}$$

The production cross section of this process, which is widely dominated by resonant Z bosons, is large, and the final state of the hard-scattering process is completely reconstructable. When the transverse momentum of the jet is large, the dilepton pair will be boosted, and the process provides a source for high-energy lepton pairs with opposite charge (opposite-sign lepton pairs). The invariant-mass distribution of the leptons is dominated by the Z-boson resonance, and a good theoretical understanding of this resonance also for boosted Z bosons is a cornerstone of an efficient detector calibration. Providing high-energy lepton pairs and jet(s), Z + jet(s) production is not only a Standard Model (SM) candle process but also an important background for new-physics searches. Moreover, the process offers the possibility for precision tests of jet dynamics in QCD.

The importance of Drell–Yan processes is also reflected in the effort to make the theoretical predictions as precise as possible. The differential cross section for W/Z production is known at next-to-next-to-leading order (NNLO) accuracy (i.e. at two loops) with respect to QCD corrections [3] and even up to N^{3}LO in the soft-plus-virtual approximation [4]. The next-to-leading-order (NLO) QCD corrections have been matched with parton showers [5] and combined with a summation of soft-gluon radiation (see e.g. Ref. [6]), which is necessary to predict the transverse-momentum distribution of the EW bosons for small p_{T}. In view of QCD only, the neutral- and charged-current Drell–Yan processes are very similar. However, concerning EW corrections, the production of W and Z bosons show considerable differences and have been addressed separately. The NLO EW corrections are known for the charged-current [7–10] as well as the neutral-current process [11–13] and the predictions have been refined in various ways, e.g. upon including multi-photon radiation [10,13–16], photon-induced processes [12,13,16–18], and EW corrections within the MSSM [13, 16]. Also the interplay of QCD and EW effects has been investigated [19].

The cross sections for W/Z + 1 jet [20–22] and W/Z + 2 jets [21] production at NLO QCD are known for a long time. Recently, NLO QCD results for W/Z + 3 jets and even W + 4 jets production (in leading-colour approximation) were presented [23]. W/Z + 1 jet production has also been matched with parton showers [24]. In the EW sector, higher-order corrections to W + 1 jet production have been first analyzed in the on-shell approximation [25–27] and later extended to the full NLO EW corrections for the physical final state [28], i.e. a charged lepton, a neutrino, and a hard jet.

As far as EW corrections to Z + 1 jet production are concerned, only the purely weak one-loop corrections in the SM have been investigated in the on-shell approximation [29, 30], i.e. in this calculation the Z boson is treated as a stable external particle and photonic corrections have been ignored. For Z bosons at large transverse momentum, requiring a large centre-of-mass energy, using on-shell Z bosons is a good approximation since the EW corrections are dominated by large universal Sudakov logarithms [31]. In Ref. [29] the leading corrections up to the next-to-leading logarithms at the one- and two-loop level have been calculated. Later the full NLO weak corrections have been added [30]. However, the on-shell calculation is limited to a particular kinematic regime where neither off-shell effects nor the event definition for the physical final state play a role. Finally, photonic corrections have to be taken into account for a precision at the level of a couple of percent.

In this work, we present a calculation of the NLO (i.e. one-loop) EW corrections for the physical final state, i.e. for the process $\mathrm{pp/p\bar{p}} \to l^+l^- + \mathrm{jet} + X$. Following our earlier work [28] on W + 1 jet production, the Z-boson resonance is described in the complex-mass scheme [32,33]. All off-shell effects due to the finite width of the Z boson, the contributions of and the interference with an intermediate photon, and photonic corrections are included. Our results have been implemented in a fully flexible Monte Carlo code which is able to calculate binned distributions for all physically relevant Z + 1 jet observables. In real emission events with photons inside a jet, we distinguish Z + jet and Z + photon production by a cut on the photon energy fraction inside the jet employing a measured quark-to-photon fragmentation function [34].

Our calculation is completely generic and thus not limited to specific observables or kinematic regimes. The interplay between the (potentially resonant) Z boson and the off-shell photon is included without approximations at NLO and can also be studied for observables for which the exchanged Z boson is far off shell and the photon contribution is potentially sizeable. However, we rely on the presence of a hard jet with sizable transverse momentum in the final state. For final-state jets which become soft or collinear to the beam pipe, the calculation breaks down. Nevertheless, the calculation of the EW corrections for Z production in association with a hard jet is also a step towards the mixed NNLO EW and QCD corrections to inclusive Z-boson production.

We have also recalculated the NLO QCD corrections at $\mathcal{O}(\alpha^2\alpha_s^2)$ in a fully flexible way, supporting a phase-space dependent choice for the factorization and renormalization scales, as will be discussed in some detail in Section 3.

This paper is organized as follows. In Section 2, we describe our calculation in detail and discuss all the theoretical concepts and tools which have been used. In Section 3, we specify the numerical input as well as the details of our event selection. Numerical results are given for Z + jet production both at the LHC and at the Tevatron. We present inclusive cross sections for specified sets of cuts as well as distributions for the relevant observables. Our conclusions are given in Section 4.

2 Details of the calculation

2.1 General setup

At hadron colliders, the production of a charged-lepton pair via Z-boson or photon exchange in association with one hard jet is governed at leading order (LO) by quark–antiquark fusion, where the initial-state quarks radiate a gluon, and the corresponding crossed channels with a gluon in the initial state. To be specific, the relevant partonic processes are

$$q_i\ \bar{q}_i \to \mathrm{Z}/\gamma^*\mathrm{g} \to l^+l^-\ \mathrm{g}\,, \tag{2.1}$$

$$q_i\ \mathrm{g} \to \mathrm{Z}/\gamma^* q_i \to l^+l^-\ q_i\,, \tag{2.2}$$

$$\bar{q}_i\ \mathrm{g} \to \mathrm{Z}/\gamma^* \bar{q}_i \to l^+l^-\ \bar{q}_i\,, \tag{2.3}$$

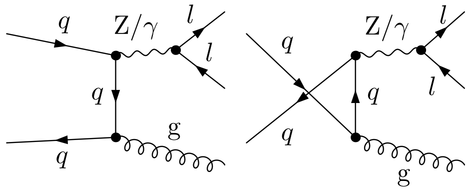

Figure 1: Feynman diagrams for the LO process (2.1).

where q_i denotes any light quark, i.e. $q_i = \mathrm{u, d, c, s, b}$. The corresponding tree-level Feynman diagrams for process (2.1) are shown in Figure 1. The intermediate Z-boson resonance is described by a complex Z-boson mass μ_Z via the replacement

$$M_\mathrm{Z}^2 \to \mu_\mathrm{Z}^2 = M_\mathrm{Z}^2 - \mathrm{i} M_\mathrm{Z} \Gamma_\mathrm{Z} \tag{2.4}$$

in the Z propagator as dictated by the complex-mass scheme (see below). Hence, all our results correspond to a fixed-width description of the Breit–Wigner resonance. Moreover, all related quantities, in particular the weak mixing angle, have to be formulated in terms of the complex mass parameters. The final-state leptons are treated as massless unless their small masses are used to regularize a collinear divergence.

The tree-level amplitudes do not depend on the quark generation and only differ for up- and down-type quarks due to the different quantum numbers in the $\mathrm{Z}q\bar{q}$ vertex. Hence, the summation over the quark flavours is straightforward for each of the three process types shown in (2.1)–(2.3) when folding the squared tree-level amplitudes with the corresponding PDFs. The five quark flavours (including the bottom quark), which appear as external particles, are treated as massless throughout the calculation, except if small masses are used to regularize a collinear divergence. At tree level the bottom-quark-induced processes do not show any peculiarities. Only in the evaluation of the EW virtual corrections they have to be treated with special care (see Section 2.2).

In this work, we describe $\mathrm{Z} + \mathrm{jet}$ production at NLO accuracy w.r.t. EW contributions, i.e. at the order $\mathcal{O}(\alpha^3 \alpha_\mathrm{s})$. Hence, we also include the tree-level processes with a photon in the initial state,

$$q_i\, \gamma \to \mathrm{Z}/\gamma^* q_i \to l^+ l^-\, q_i\,, \tag{2.5}$$

$$\bar{q}_i\, \gamma \to \mathrm{Z}/\gamma^* \bar{q}_i \to l^+ l^-\, \bar{q}_i\,, \tag{2.6}$$

which contribute at the order $\mathcal{O}(\alpha^3)$ and may thus lead to relevant corrections at the expected accuracy level of a few percent. The tree-level Feynman diagrams for process (2.5) are shown in Figure 2. The photon content of the proton has been quantified in the MRSTQED2004 PDFs [35]. Since the photon also couples to the charged leptons in the final state, the amplitude is more involved than its QCD counterpart. As in our earlier work on $\mathrm{W} + \mathrm{jet}$ production, in this work, we do not consider the crossed processes corresponding to $l^+l^- + \mathrm{photon}$ production, which would lead to tiny corrections. The non-trivial definition and separation of the $l^+l^- + \mathrm{jet}$ and $l^+l^- + \mathrm{photon}$ final states when additional photons are present due to bremsstrahlung are discussed in detail in Section 2.3.

To complete the description of the general setup of our calculation, we also repeat a few points which do not differ from our earlier calculation for $\mathrm{W} + \mathrm{jet}$ production. To define the

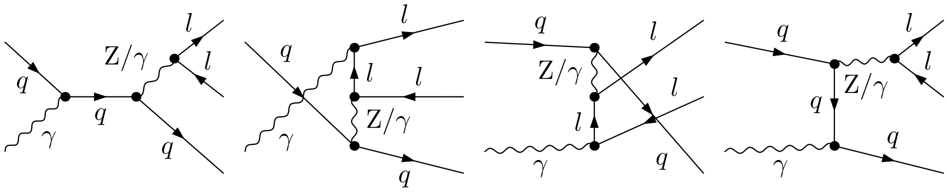

Figure 2: Feynman diagrams for the photon-induced process (2.5).

electromagnetic coupling constant α, we use the G_μ scheme, i.e. we derive α from the Fermi constant according to

$$\alpha_{G_\mu} = \frac{\sqrt{2} G_\mu M_{\mathrm{W}}^2}{\pi} \left(1 - \frac{M_{\mathrm{W}}^2}{M_{\mathrm{Z}}^2}\right). \tag{2.7}$$

In this scheme, the weak corrections to muon decay Δr are included in the charge renormalization constant (see e.g. Ref. [8]). As a consequence, the EW corrections are independent of logarithms of the light-quark masses. Moreover, this definition effectively resums the contributions associated with the running of α from zero to the weak scale and absorbs some leading universal corrections $\propto G_\mu m_{\mathrm{t}}^2$ from the ρ parameter into the LO amplitude.

For corrections due to collinear final-state radiation it would be more appropriate to use $\alpha(0)$ defined in the Thomson limit to describe the corresponding coupling. On the other hand, using α_{G_μ} everywhere is best suited to describe the large corrections due to Sudakov logarithms in the high-energy regime. Thus, the optimal choice cannot be achieved in one particular input scheme, and necessarily the calculation requires more refinements beyond NLO. In particular, among other things, higher-order effects from multi-photon emission should also be included at this level of precision which is beyond the scope of this work. We find that the difference of the two schemes in an NLO calculation only amounts to about 3% of the EW corrections.

We employ the traditional Feynman-diagrammatic approach to calculate all relevant amplitudes in the 't Hooft–Feynman gauge. For a numerical evaluation at the amplitude level we use the Weyl–van-der-Waerden spinor formalism. To ensure the correctness of the presented results we have performed two independent calculations which are in mutual agreement.

One calculation starts from diagrammatic expressions for the one-loop corrections generated by FeynArts 1.0 [36]. The algebraic evaluation of the loop amplitudes is performed with an in-house program written in *Mathematica*, and the results are automatically transferred to *Fortran*. The Born and bremsstrahlung amplitudes are calculated and optimized by hand and directly included into a *Fortran* program for numerical evaluation. A specific parametrization of phase space is used for an adaptive Monte Carlo integration employing the Vegas [37] algorithm.

The second calculation is based on FeynArts 3.2 [38] and FormCalc version 3.1 [39]. The translation of the amplitudes into the Weyl–van-der-Waerden formalism as presented in Ref. [40] is performed with the program Pole [41]. Pole also provides an interface to the multi-channel phase-space integrator Lusifer [42] which has been extended to use Vegas in order to optimize each phase-space mapping. Madgraph [43] has been very useful for internal checks of the real-emission amplitudes.

2.2 Virtual corrections

We calculate the virtual one-loop QCD and EW corrections for the partonic processes (2.1)–(2.3), but do not include the NLO QCD corrections to the photon-induced processes which are formally part of the corrections up to $\mathcal{O}(\alpha^3\alpha_s)$. The cross section of the photon-induced processes turns out to be numerically small at LO, and the corresponding corrections in the case of W + jet production turned out to be completely negligible. Hence, we do not expect phenomenologically relevant corrections for Z + jet either. We do not include the (loop-induced) contributions of the partonic process $gg \to Z\,g$. Based on Ref. [22] its contribution at the LHC and the Tevatron can be estimated to be below one percent.

The calculated virtual QCD corrections are straightforward to implement and consist of up to box (4-point) diagrams only. The NLO EW corrections are more involved and additionally include pentagon (5-point) diagrams. There are $\mathcal{O}(200)$ diagrams per partonic channel, including 9 pentagons and 32 boxes. The general structure of the contributions is completely equivalent to our earlier work on W + jet production. However, Z + jet is computationally more demanding, not only because there are more diagrams per partonic channel but also because there are more helicity combinations contributing to the cross section which are summed at each phase-space point. The generic structure of the contributing diagrams is indicated in Figure 3, and the pentagon diagrams are explicitly given in Figure 4. The different channels are related by crossing symmetry.

Concerning the EW corrections, the partonic processes with one or two (anti-) bottom quarks in the initial state play a special role: There are box and pentagon diagrams with two W bosons and a heavy top quark in the loop. For all other partonic processes, only massless quarks propagate in the loops because we neglect CKM mixing, i.e. we set the CKM matrix to unity in our calculation. The mass of the top quark shifts the total EW correction roughly by a per mille for the most inclusive cross section discussed in Section 3.

The potentially resonant Z bosons require a proper inclusion of the finite gauge-boson width in the propagators. We use the complex-mass scheme, which was introduced in Ref. [32] for LO calculations and generalized to the one-loop level in Ref. [33]. In this approach the W- and Z-boson masses are consistently treated as complex quantities, defined as the locations of the propagator poles in the complex plane. This leads to complex couplings and, in particular, a complex weak mixing angle. The scheme fully respects all relations that follow from gauge invariance. A brief description of the complex-mass scheme can also be found in Ref. [44].

The amplitudes can be expressed in terms of "standard matrix elements" [45], which comprise all polarization-dependent quantities (spinor chains, polarization vectors), and invariant coefficients, which contain the tensor integrals. The tensor integrals are recursively reduced to master integrals at the numerical level. The standard scalar integrals are evaluated using two in-house *Fortran* libraries which are based on the results of Ref. [46] for 4-point functions with complex internal masses and on the methods and results of Ref. [47]. Results for different regularization schemes are translated into each other with the method of Ref. [48]. Tensor and scalar 5-point functions are directly expressed in terms of 4-point integrals [49–51], while tensor 4-point and 3-point integrals are recursively reduced to scalar integrals with the Passarino–Veltman algorithm [52]. Although we already find sufficient numerical stability with this procedure, we additionally apply the dedicated expansion methods of Ref. [51] in exceptional phase-space regions where small Gram determinants appear.

UV divergences are regularized dimensionally. For the infrared (IR), i.e. soft or collinear, divergences we either use pure dimensional regularization with massless gluons, photons, and fermions (except for the top quark), or alternatively pure mass regularization with infinitesimal photon, gluon, and small fermion masses, which are only kept in the mass-singular logarithms. When using dimensional regularization, the rational terms of IR origin are treated as described in Appendix A of Ref. [53]; the ones of UV origin are always automatically included in the amplitude and tensor integral reduction.

Self-energy insertions:

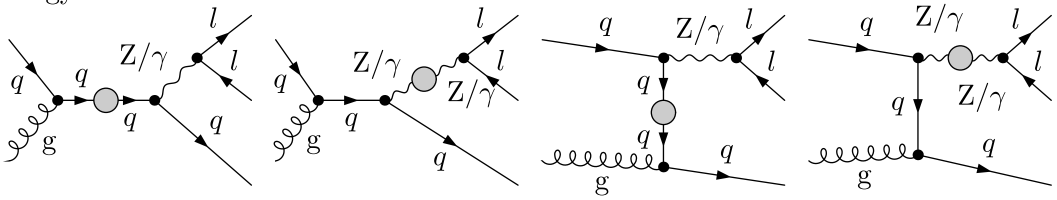

Triangle insertions:

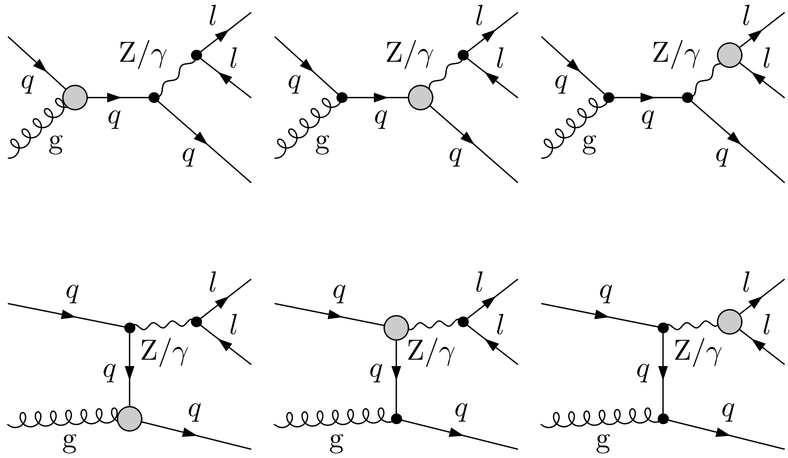

Box and pentagon insertions:

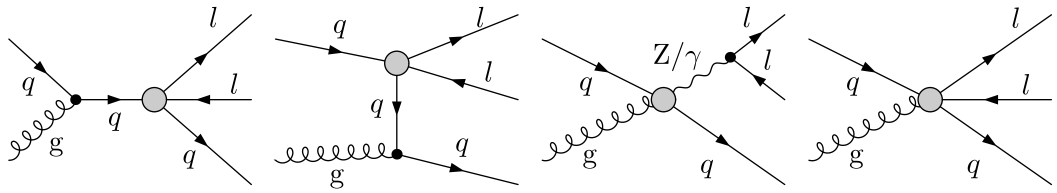

Figure 3: Contributions of different one-particle irreducible vertex functions (indicated as blobs) to the LO process (2.2); there are contributions from self-energies, triangles, boxes, and pentagon graphs.

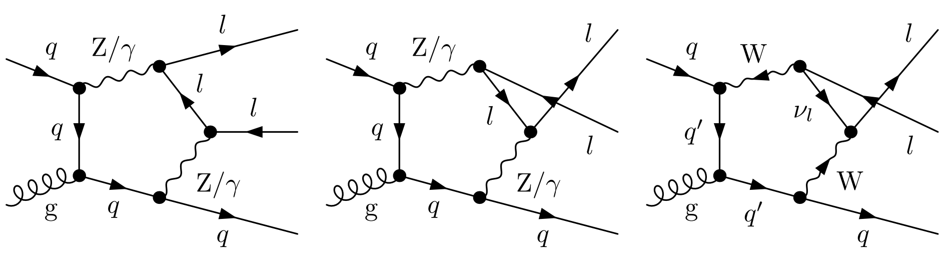

Figure 4: Virtual pentagon contributions to the process (2.2). Note that for external bottom quarks the exchange of two W bosons leads to diagrams with massive top-quark lines ($q' = \text{top}$) in the loop.

We use an on-shell renormalization prescription for the EW part of the SM as detailed in Ref. [33] for the complex-mass scheme. Employing the G_μ scheme for the definition of the fine-structure constant α, we include Δr in the charge renormalization constant as mentioned above. The strong coupling constant is renormalized in the $\overline{\mathrm{MS}}$ scheme with five active flavours. Hence, bottom quarks are included everywhere in the calculation as a massless quark flavour.

2.3 Real corrections

The evaluation of the real corrections has to be done with particular care, both for theoretical consistency as well as to match the experimental observables as closely as possible. Let us first focus on the EW real corrections to the partonic processes (2.1)–(2.3). The emission of an additional photon leads to the processes

$$
\begin{aligned}
q_i\ \bar{q}_i &\to l^+ l^-\ \mathrm{g}\,\gamma\,, && (2.8)\\
q_i\ \mathrm{g} &\to l^+ l^-\ q_i\,\gamma\,, && (2.9)\\
\bar{q}_i\ \mathrm{g} &\to l^+ l^-\ \bar{q}_i\,\gamma\,. && (2.10)
\end{aligned}
$$

The Feynman diagrams contributing to the process (2.9) are shown in Figure 5. Due to the emission of soft photons the real corrections include soft singularities which are cancelled by corresponding contributions in the virtual corrections independently of the details of the event selection or recombination procedure. If the photon and the charged leptons/quarks are recombined into a pseudo-particle (mimicking the start of hadronic or electromagnetic showers) to form IR-safe observables, all the remaining singularities arising from collinear photon emission in the final state also cancel against the corresponding singularities in the virtual corrections. This requires that all the selection cuts for a given observable are blind to the distribution of momenta in collinear lepton–photon configurations. The left-over collinear singularities due to collinear photon emission off the initial-state quarks are absorbed by a redefinition of the PDFs. Technically, we use the dipole subtraction formalism as specified for photon emission in Refs. [54, 55] to isolate all the divergences and ensure the numerical cancellation.

Note that only the MRSTQED2004 PDFs properly account for all QED effects at NLO. However, this PDF set is outdated by now and does not include many modern PDF developments. Hence, we only employ the MRSTQED2004 set to estimate the photon content of the proton and use more modern sets for all the partonic channels without photons in the initial state. In a strict sense, with the choice of a modern PDF set the calculation is not fully consistent (like a NLO QCD calculation employing a LO PDF set). However, the numerical effect from a proper inclusion of the NLO EW corrections in the PDF determination is expected to be small, since this was also the case for the MRSTQED2004 fit when compared to the corresponding fit neglecting QED effects. The MRSTQED2004 PDF was defined in the DIS scheme so we stick to this scheme in our calculation.

For muons in the final state it is experimentally possible to separate collinear photons from the lepton, i.e. to observe so-called “bare” muons. On the theoretical side, this corresponds to the fact that the lepton mass cuts off the collinear divergence in a physically meaningful way. Hence, the corresponding collinear singularities show up as logarithms of the small lepton (muon) mass since the KLN theorem [56] does not apply to non-collinear-safe observables. Our treatment and the analytical extraction of these collinear mass logarithms using the algorithm of Ref. [55] has been explained in detail in Ref. [28]. For $\mathrm{Z}+\mathrm{jet}$ production, there are of course two charged leptons in the final state which can emit collinear photons. Apart from this straightforward generalization, which simply leads to more dipole subtraction terms, the same formalism applies.

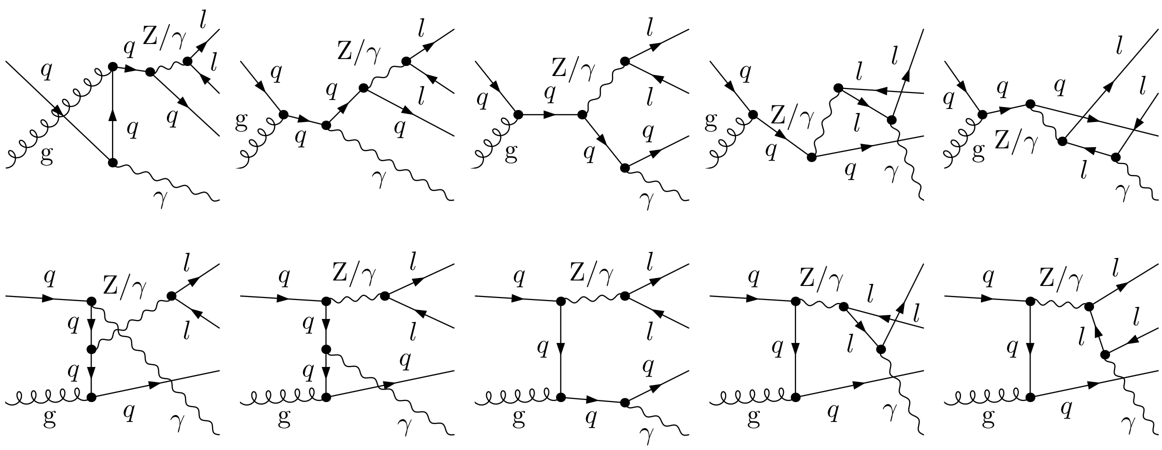

Figure 5: Real photonic bremsstrahlung corrections to the LO process (2.2).

As in all processes with jets in the final state, the inclusion of EW corrections to Z + jet production asks for a precise event definition in order to distinguish Z +jet from Z+γ production. We follow the strategy used for W+jet production which is detailed in Refs. [28,57]: We exclude jets which primarily consist of a hard photon (see Section 3) and capture the non-perturbative physics in the collinear quark–photon splittings [58] by means of the measured fragmentation function [34].

Concerning the real corrections in NLO QCD, there are no particular complications when all the contributing partonic channels are identified. An additional gluon leads to the processes

$$q_i\ \bar{q}_i \to l^+l^-\,\mathrm{g}\,\mathrm{g}\,, \tag{2.11}$$
$$q_i\ \mathrm{g} \to l^+l^-\,q_i\,\mathrm{g}\,, \tag{2.12}$$
$$\bar{q}_i\ \mathrm{g} \to l^+l^-\,\bar{q}_i\,\mathrm{g}\,, \tag{2.13}$$
$$\mathrm{g}\ \mathrm{g} \to l^+l^-\,\bar{q}_i\,q_i\,. \tag{2.14}$$

Furthermore, the gluon present at LO may split into two quarks, inducing the processes

$$q_i\ \bar{q}_i \to l^+l^-\,q_i\,\bar{q}_i\,, \tag{2.15}$$
$$q_i\ \bar{q}_i \to l^+l^-\,q_j\,\bar{q}_j \quad (q_i \neq q_j)\,, \tag{2.16}$$
$$q_i\ \bar{q}_j \to l^+l^-\,q_i\,\bar{q}_j \quad (q_i \neq q_j)\,, \tag{2.17}$$
$$\bar{q}_i\ \bar{q}_i \to l^+l^-\,\bar{q}_i\,\bar{q}_i\,, \tag{2.18}$$
$$\bar{q}_i\ \bar{q}_j \to l^+l^-\,\bar{q}_i\,\bar{q}_j \quad (q_i \neq q_j)\,, \tag{2.19}$$
$$q_i\ q_i \to l^+l^-\,q_i\,q_i\,, \tag{2.20}$$
$$q_i\ q_j \to l^+l^-\,q_i\,q_j \quad (q_i \neq q_j)\,, \tag{2.21}$$

where q_i denotes again quarks of the five light flavours. Note that different Feynman diagrams contribute for $i = j$ and $i \neq j$, so we list the corresponding partonic processes separately. Taking this difference into account, as well as the correct quantum numbers for up- and down-type quarks, the remaining sums over flavour can again efficiently be performed when convoluting the squared matrix elements with PDFs. As in the EW case, we use the dipole subtraction method [59] to extract the IR singularities analytically from the numerical phase-space integration. Absorbing all the collinear singularities due to initial-state splittings into the relevant

PDFs, the remaining collinear and soft divergences cancel all the divergences of the one-loop QCD corrections for processes (2.1)–(2.3). As explained already in Section 2.2, we do not include the NLO QCD corrections to the photon-induced processes.

For the six-fermion processes (2.15), (2.18), and (2.20) with identical fermions, diagrams with gluon exchange can interfere with purely EW diagrams at $\mathcal{O}(\alpha^3\alpha_s)$. The result is non-singular in the collinear limits due to the restrictions from colour flow, but in contrast to the other subprocesses with different quark flavours it does not vanish. However, the effect of this non-trivial interference contribution is expected to be phenomenologically negligible, as shown for the similar process W + jet production in Ref. [28]. Therefore, we neglect these contributions in our numerical analysis.

3 Numerical results

3.1 Input parameters and setup

The relevant SM input parameters are

$$\begin{aligned}
G_\mu &= 1.16637\times10^{-5}\,\mathrm{GeV}^{-2}, & \alpha_s(M_Z) &= 0.1202, & & \\
M_W^{OS} &= 80.398\,\mathrm{GeV}, & \Gamma_W^{OS} &= 2.141\,\mathrm{GeV}, & & \\
M_Z^{OS} &= 91.1876\,\mathrm{GeV}, & \Gamma_Z^{OS} &= 2.4952\,\mathrm{GeV}, & M_H &= 120\,\mathrm{GeV}, \\
m_e &= 0.510998910\,\mathrm{MeV}, & m_\mu &= 105.658367\,\mathrm{MeV}, & m_t &= 172.6\,\mathrm{GeV},
\end{aligned} \tag{3.1}$$

which essentially follow Ref. [60]. As stated before, the CKM matrix only appears in loops and is set to unity, because its effect is negligible there.

Using the complex-mass scheme [33], we employ a fixed width in the resonant W- and Z-boson propagators in contrast to the approach used at LEP and Tevatron to fit the W and Z resonances, where running widths are taken. Therefore, we have to convert the "on-shell" (OS) values of M_V^{OS} and Γ_V^{OS} ($V = \mathrm{W, Z}$), resulting from LEP and Tevatron, to the "pole values" denoted by M_V and Γ_V. The relation between the two sets of values is given by [61]

$$M_V = M_V^{OS}/\sqrt{1+(\Gamma_V^{OS}/M_V^{OS})^2}, \qquad \Gamma_V = \Gamma_V^{OS}/\sqrt{1+(\Gamma_V^{OS}/M_V^{OS})^2}, \tag{3.2}$$

leading to

$$\begin{aligned}
M_W &= 80.370\ldots\ \mathrm{GeV}, & \Gamma_W &= 2.1402\ldots\ \mathrm{GeV}, \\
M_Z &= 91.153\ldots\ \mathrm{GeV}, & \Gamma_Z &= 2.4943\ldots\ \mathrm{GeV}.
\end{aligned} \tag{3.3}$$

We make use of these mass and width parameters in the numerics discussed below, although the difference between using M_V or M_V^{OS} would be hardly visible.

As explained in Section 2.1, we adopt the G_μ scheme, where the electromagnetic coupling α is set to α_{G_μ}. In this scheme the electric-charge renormalization constant does not contain logarithms of the light-fermion masses, in contrast to the $\alpha(0)$ scheme, so that the results become practically independent of the light-quark masses.

We use the central MSTW2008NLO PDF set [62] in its LHAPDF implementation [63] for our numerical results. This implies the value of $\alpha_s(M_Z)$ stated in (3.1). We use the α_s running as provided by the LHAPDF collaboration. Only the photon-induced processes are evaluated with the MRSTQED2004 set of PDFs [35] as discussed in Section 2.3. Here, we use the corresponding value of $\alpha_s(M_Z) = 0.1190$.

The QCD and QED factorization scales as well as the renormalization scale are always identified. For low-p_{T} jets, the scale of the process is given by the invariant mass of the leptons which in turn peaks around M_{Z} for resonant Z-boson production. Hence, one natural choice is the Z-boson mass, i.e. $\mu_{\mathrm{R}} = \mu_{\mathrm{F}} = M_{\mathrm{Z}}$. For high-$p_{\mathrm{T}}$ jets, well beyond the Z-mass scale, however, the relevant scale is certainly larger, and the QCD emission from the initial state is best modelled by the p_{T} of the jet itself (see e.g. Ref. [64]). To interpolate between the two regimes, we alternatively use

$$\mu = \mu_{\mathrm{R}} = \mu_{\mathrm{F}} = \sqrt{M_{\mathrm{Z}}^2 + (p_{\mathrm{T}}^{\mathrm{had}})^2} \tag{3.4}$$

as a phase-space dependent scale, where $p_{\mathrm{T}}^{\mathrm{had}}$ is given by the p_{T} of the summed four-momenta of all partons, i.e. quarks and/or gluons, in the final state. At LO, $p_{\mathrm{T}}^{\mathrm{had}}$ is simply the p_{T} of the one final-state jet. We present numerical results for both scale choices.

3.2 Phase-space cuts and event selection

In order to define IR-safe observables for the process $\mathrm{pp/p\bar{p}} \to \mathrm{Z}/\gamma^* + \mathrm{jet} \to l^+l^- + \mathrm{jet} + X$ we recombine final-state partons and photons to pseudo-particles and impose a set of phase-space cuts as detailed in the following subsections.

3.2.1 Recombination

To define the recombination procedure and the separation cuts, we use the variables $R_{ij} = \sqrt{(y_i - y_j)^2 + \phi_{ij}^2}$, where y_i denotes the rapidity $y = \frac{1}{2}\ln[(E + p_{\mathrm{L}})/(E - p_{\mathrm{L}})]$ of particle i and ϕ_{ij} is the azimuthal angle in the transverse plane between the particles i and j. In the definition of the rapidity, E denotes the particle's energy and p_{L} its three-momentum along the beam axis. The recombination procedure, where we simply add four-momenta to form a pseudo-particle, works as follows:

1. For observables with bare muons we do not recombine photons and leptons. For inclusive observables, a photon and a lepton are recombined for $R_{\gamma l} < 0.1$. If both charged leptons in the final state are close to the photon we recombine it with the lepton leading to the smallest $R_{\gamma l}$.

2. A photon and a parton a (quark or gluon) are recombined for $R_{\gamma a} < 0.5$. In this case, we use the energy fraction of the photon inside the jet, $z_\gamma = E_\gamma/(E_\gamma + E_a)$, to distinguish between $\mathrm{Z} + \mathrm{jet}$ and $\mathrm{Z} + \gamma$ production. If $z_\gamma > 0.7$, the event is regarded as a part of $\mathrm{Z} + \gamma$ production and rejected because it lacks any other hard jet at NLO. This event definition is not collinear safe and requires the use of quark-to-photon fragmentation functions to include the non-perturbative part of the quark–photon splitting as mentioned in Section 2.3. Our results are not very sensitive to the specific choice of the cut on z_γ.

3. Two partons a, b are recombined for $R_{ab} < 0.5$. For our simple final-state configurations, this procedure is equivalent to the Tevatron Run II k_{T}-algorithm [65] for jet reconstruction with resolution parameter $D = 0.5$.

Technically, we perform a possible photon–lepton recombination before the photon–parton recombination. This procedure is IR safe because the triple-soft/collinear situation that a photon should have been first recombined with a parton, but was erroneously first recombined with a lepton, is excluded by our basic cuts.

3.2.2 Basic cuts

After applying the recombination procedure of the previous section we define $\mathrm{Z}+\mathrm{jet}$ events by the following basic cuts:

1. A partonic object (after a possible recombination) is called a jet if its transverse momentum p_T is larger than $p_{\mathrm{T,jet}}^{\mathrm{cut}} = 25\,\mathrm{GeV}$. Events are required to include at least one jet.

2. We demand two charged leptons with transverse momenta $p_{\mathrm{T},l} > 25\,\mathrm{GeV}$.

3. The events have to be central, i.e. the leptons and at least one jet have to be produced in the rapidity range $|y| < y_{\mathrm{max}} = 2.5$.

4. The leptons have to be isolated, i.e. the event is discarded if the distance between one of the leptons and a jet $R_{l\mathrm{jet}}$ is smaller than 0.5. The lepton–jet separation is also required for jets with $|y| > y_{\mathrm{max}}$.

   Note in addition that it is important to exclude low-p_T partons from the lepton–jet separation procedure (guaranteed by step 1.), since otherwise observables would not be IR safe.

While the EW corrections differ for final-state electrons and muons without photon recombination, the corrections become universal in the presence of photon recombination, since the lepton-mass logarithms cancel in this case, in accordance with the KLN theorem. Numerical results are presented both for photon recombination and for bare muons.

For certain observables, we apply a jet veto against a second hard jet. To be specific, we veto any sub-leading jet with $p_\mathrm{T} > p_{\mathrm{T,j_1}}/2$, where $p_{\mathrm{T,j_1}}$ denotes the p_T of the "leading" jet, i.e. the one with maximal p_T.

3.3 Results on cross sections and distributions

We consider the production of a lepton pair in association with a jet at the Tevatron, i.e. for a $\mathrm{p\bar{p}}$ initial state with a centre-of-mass (CM) energy of $\sqrt{s} = 1.96\,\mathrm{TeV}$, and at the LHC, i.e. for a pp initial state. For the latter, we show results for $\sqrt{s} = 7\,\mathrm{TeV}$, corresponding to the available energy in the years 2010 to 2012, as well as $\sqrt{s} = 14\,\mathrm{TeV}$, the ultimate energy reach of the LHC.

We present the LO cross section σ_0 and various types of corrections δ, defined relative to the LO cross section by $\sigma = \sigma_0 \times (1+\delta)$. Concerning the EW corrections, we distinguish the cross section $\sigma_{\mathrm{EW}}^{\mu^+\mu^-}$ for bare muons and $\sigma_{\mathrm{EW}}^{\mathrm{rec}}$ for which a lepton–photon recombination is employed as defined above. Accordingly, the corresponding corrections are labelled $\delta_{\mathrm{EW}}^{\mu^+\mu^-}$ and $\delta_{\mathrm{EW}}^{\mathrm{rec}}$, respectively. An additional label specifies which renormalization and factorization scale is used. Either we use the fixed scale ($\mu = M_\mathrm{Z}$) or we determine the scale on an event-by-event basis by the kinematical configuration of the final state (var), as specified in (3.4). For the EW corrections the difference is small, since the LO and the NLO results depend on the renormalization scale for α_s and the QCD factorization scale in the same way. However, for the QCD part a sensible scale choice can be crucial for the stability of the perturbative series. Accordingly, the QCD corrections are labelled $\delta_{\mathrm{QCD}}^{\mu=M_\mathrm{Z}}$ for a fixed scale choice and $\delta_{\mathrm{QCD}}^{\mathrm{var}}$ for the scale choice defined in (3.4).

As already observed for W+jet production in Ref. [28] and shown below, the QCD corrections become larger and larger with increasing p_T of the leading jet. The increase in the cross section results from a new kinematical configuration which is available for the $\mathrm{Z}+2\,\mathrm{jets}$ final state. The large p_T of the leading jet is not balanced by the leptons, as required at LO, but by the second jet.

$p_{\mathrm{T,jet}}/\,\mathrm{GeV}$	$25-\infty$	$50-\infty$	$100-\infty$	$200-\infty$	$500-\infty$	$1000-\infty$
$\sigma_0^{\mu=M_\mathrm{Z}}/\,\mathrm{fb}$	123491(7)	44603(2)	11364.4(5)	1813.26(8)	64.120(2)	2.11859(6)
$\sigma_0^{\mathrm{var}}/\,\mathrm{fb}$	122024(7)	43254(2)	10445.0(4)	1475.76(6)	38.648(1)	0.90847(3)
$\delta_{\mathrm{EW}}^{\mu^+\mu^-,\mathrm{var}}/\%$	-4.2	-4.5	-5.1	-8.5	$-17.4(1)$	$-27.0(1)$
$\delta_{\mathrm{EW}}^{\mathrm{rec},\mathrm{var}}/\%$	-2.8	-3.2	-4.2	-7.8	$-16.7(1)$	$-26.3(1)$
$\delta_{\mathrm{QCD}}^{\mu=M_\mathrm{Z}}/\%$	35.8(1)	48.7(1)	63.9(1)	86.9(1)	142.6(1)	210.5(1)
$\delta_{\mathrm{QCD}}^{\mathrm{var}}/\%$	35.9(1)	50.1(1)	70.0(1)	107.0(1)	217.3(1)	403.8(1)
$\delta_{\mathrm{QCD,veto}}^{\mu=M_\mathrm{Z}}/\%$	13.1(1)	9.8(1)	14.1(1)	13.4(1)	$-2.4(1)$	$-29.1(1)$
$\delta_{\mathrm{QCD,veto}}^{\mathrm{var}}/\%$	14.1(1)	12.6(1)	21.9(1)	32.3(1)	44.8(1)	54.2(1)
$\delta_{\gamma}^{\mathrm{var}}/\%$	0.1	0.2	0.2	0.4	0.6	1.0
$\sigma_{\mathrm{full,veto}}^{\mu^+\mu^-,\mathrm{var}}/\,\mathrm{fb}$	134266(49)	46852(20)	12223(4)	1832.5(8)	49.45(2)	1.1649(7)

Table 1: Integrated cross sections for different cuts on the p_{T} of the leading jet (jet with highest p_{T}) at the LHC with $\sqrt{s} = 14\,\mathrm{TeV}$. We show the LO results both for a variable and for a constant scale. The relative EW corrections δ_{EW} are given with and without lepton–photon recombination. The QCD corrections δ_{QCD} are presented for a fixed as well as a for variable scale and with or without employing a veto on a second hard jet. The EW corrections and the corrections due to photon-induced processes, δ_γ, are presented for the variable scale. Finally, we show the full NLO cross section $\sigma_{\mathrm{full,veto}}^{\mu^+\mu^-,\mathrm{var}}$. The error from the Monte Carlo integration for the last digit(s) is given in parenthesis as far as significant. See text for details.

Hence, we encounter the production of 2 jets where one of the quark lines radiates a relatively soft Z boson or off-shell photon. This part of the cross section, which does not really correspond to a true NLO correction to Z + jet production, can be separated by employing a veto against a second hard jet in real-emission events. Hence, we present NLO QCD corrections with a jet veto ($\delta_{\mathrm{QCD,veto}}^{\mu=M_\mathrm{Z}}$, $\delta_{\mathrm{QCD,veto}}^{\mathrm{var}}$) and without a jet veto ($\delta_{\mathrm{QCD}}^{\mu=M_\mathrm{Z}}$, $\delta_{\mathrm{QCD}}^{\mathrm{var}}$).

Using a jet veto based on a fixed p_{T} value for the second jet is not well suited. It will either cut away relatively collinear emission events in the high-p_{T} tails of the leading-jet distribution (leading to large negative corrections) or it has to be chosen too large to be effective in the intermediate-p_{T} parts of the distribution. Hence, building on our experience from W + jet production, we apply the jet veto defined at the end of Section 3.2.2. We have checked that this jet veto indeed effectively removes events with back-to-back jet kinematics.

We also investigate the impact of the photon-induced tree-level processes (2.5) and (2.6). Since the LO photon-induced cross section is a small effect, we show its relative impact δ_γ with respect to the LO cross section at $\mathcal{O}(\alpha^2\alpha_{\mathrm{s}})$ where initial states with photons are not taken into account. The NLO QCD corrections to these channels as well as the interference contributions discussed at the end of Section 2.3 are neglected in the following.

In Tables 1–6 we show the LO integrated cross sections, the corresponding relative corrections introduced above, and the NLO cross section $\sigma_{\mathrm{full,veto}}^{\mu^+\mu^-,\mathrm{var}}$ including the EW corrections for bare

$\mathrm{pp} \to l^+l^-\,\mathrm{jet} + X$ at $\sqrt{s} = 7\,\mathrm{TeV}$

$p_{\mathrm{T,jet}}/\,\mathrm{GeV}$	$25-\infty$	$50-\infty$	$100-\infty$	$200-\infty$	$500-\infty$	$1000-\infty$
$\sigma_0^{\mu=M_\mathrm{Z}}/\,\mathrm{fb}$	53029(3)	17736.0(5)	3939.51(9)	471.85(1)	7.4538(2)	0.06464(6)
$\sigma_0^{\mathrm{var}}/\,\mathrm{fb}$	51949(3)	16881.3(5)	3482.85(6)	357.071(7)	3.90038(8)	0.02139(2)
$\delta_{\mathrm{EW}}^{\mu^+\mu^-,\mathrm{var}}/\%$	-4.2	-4.4	-4.9	-8.0	$-16.6(1)$	$-26.0(1)$
$\delta_{\mathrm{EW}}^{\mathrm{rec},\mathrm{var}}/\%$	-2.7	-3.1	-4.0	-7.3	$-15.9(1)$	$-25.2(1)$
$\delta_{\mathrm{QCD}}^{\mu=M_\mathrm{Z}}/\%$	35.1(1)	43.3(1)	52.2(1)	68.9(1)	119.2(1)	191.6(1)
$\delta_{\mathrm{QCD}}^{\mathrm{var}}/\%$	36.3(1)	47.0(1)	63.9(1)	100.9(1)	229.7(1)	505.0(2)
$\delta_{\mathrm{QCD,veto}}^{\mu=M_\mathrm{Z}}/\%$	15.4(1)	8.7(1)	8.9(1)	4.0(1)	$-15.3(1)$	$-44.9(1)$
$\delta_{\mathrm{QCD,veto}}^{\mathrm{var}}/\%$	17.2(1)	13.4(1)	20.7(1)	30.9(1)	48.2(1)	69.4(1)
$\delta_\gamma^{\mathrm{var}}/\%$	0.2	0.2	0.3	0.4	0.8	1.9
$\sigma_{\mathrm{full,veto}}^{\mu^+\mu^-,\mathrm{var}}/\,\mathrm{fb}$	58823(23)	18438(8)	4045(2)	440.2(2)	5.168(2)	0.03106(2)

Table 2: Integrated cross sections for different cuts on the p_T of the leading jet at the LHC with $\sqrt{s} = 7\,\mathrm{TeV}$. See caption of Table 1 and text for details.

muons, the photon-induced processes, and the QCD corrections with the jet veto for the variable scale choice for different cuts on the transverse momentum of the leading jet and the dilepton invariant mass. All other cuts and the corresponding event selection follow our default choice as introduced in Section 3.2. In Figures 6–13 we show for various observables the LO distribution and the distribution including the full set of corrections, i.e. EW corrections δ_{EW}, the contribution of the photon-induced processes δ_γ, and the QCD corrections δ_{QCD}. The various contributions to the corrections are also shown separately relative to the LO. All results are discussed in detail in the following subsections.

3.3.1 Transverse momentum of the leading jet

Tables 1–3 show the LO predictions and the above corrections for different cuts on the p_T of the leading jet $p_{\mathrm{T,jet}}$. All integrated cross sections and, hence, the corrections are dominated by events close to the lowest accepted $p_{\mathrm{T,jet}}$, as can be seen by the rapid decrease of the integrated cross section when increasing the $p_{\mathrm{T,jet}}$ cut.

For the most inclusive cross sections (left columns in the tables) the EW corrections are at the percent level and negative. With increasing $p_{\mathrm{T,jet}}$, the relevant CM energies rise, and the well-known Sudakov logarithms in the virtual EW corrections start to dominate the total corrections as expected. For $p_{\mathrm{T,jet}} \sim 1000\,\mathrm{GeV}$, the EW corrections are at the level of -25%. This behaviour is generic and also present in all other observables where the cross section is dominated by events with high CM energies.

It is evident from Tables 1 and 2 that the CM energy of the LHC plays a minor role for the EW corrections, in particular for less restrictive cuts. Since the transverse momentum of the leading jet depends only indirectly on the treatment of the lepton–photon system the corrections

$$\mathrm{p\bar{p}} \to l^+l^- \text{ jet} + X \text{ at } \sqrt{s} = 1.96\,\mathrm{TeV}$$

$p_{\mathrm{T,jet}}/\,\mathrm{GeV}$	$25-\infty$	$50-\infty$	$75-\infty$	$100-\infty$	$200-\infty$	$300-\infty$
$\sigma_0^{\mu=M_\mathrm{Z}}/\,\mathrm{fb}$	9648.3(3)	2440.3(1)	840.01(5)	340.51(2)	17.679(1)	1.3935(1)
$\sigma_0^{\mathrm{var}}/\,\mathrm{fb}$	9365.0(4)	2268.2(1)	741.47(5)	284.88(2)	12.0551(9)	0.79178(7)
$\delta_{\mathrm{EW}}^{\mu^+\mu^-,\mathrm{var}}/\%$	-4.1	-4.2	-4.0	-4.2	-6.3	-8.4
$\delta_{\mathrm{EW}}^{\mathrm{rec},\mathrm{var}}/\%$	-2.6	-2.8	-2.9	-3.3	-5.5	-7.7
$\delta_{\mathrm{QCD}}^{\mu=M_\mathrm{Z}}/\%$	30.7(1)	25.7(1)	20.3(1)	14.2(1)	$-8.7(1)$	$-31.0(1)$
$\delta_{\mathrm{QCD}}^{\mathrm{var}}/\%$	32.9(1)	31.9(1)	31.9(1)	31.8(1)	33.4(1)	33.8(1)
$\delta_{\mathrm{QCD,veto}}^{\mu=M_\mathrm{Z}}/\%$	19.8(1)	5.8(1)	0.4(1)	$-5.6(1)$	$-29.0(1)$	$-50.6(1)$
$\delta_{\mathrm{QCD,veto}}^{\mathrm{var}}/\%$	22.5(1)	12.4(1)	12.3(1)	11.4(1)	9.1(1)	7.1(1)
$\delta_\gamma^{\mathrm{var}}/\%$	0.2	0.2	0.3	0.3	0.3	0.3
$\sigma_{\mathrm{full,veto}}^{\mu^+\mu^-,\mathrm{var}}/\,\mathrm{fb}$	11102(6)	2458(2)	804(1)	306.2(3)	12.43(1)	0.784(1)

Table 3: Integrated cross sections for different cuts on the p_T of the leading jet at the Tevatron. See caption of Table 1 and text for details.

with and without recombination only slightly differ. The results for the corresponding differential distribution are shown in Figure 6 for the LHC with $\sqrt{s} = 14\,\mathrm{TeV}$ and the Tevatron.

The transverse-momentum distribution of the jet has been calculated using the approximation of a stable, on-shell Z boson in Refs. [29, 30]. Of course, in contrast to our calculation, in on-shell Z+jet production it is not possible to apply various event-selection cuts to the leptonic final state, because the degrees of freedom related to the decaying Z boson are implicitly integrated out. Nevertheless, the relative EW corrections at high momentum transfer are dominated by Sudakov logarithms of the form $\ln^2(\hat{s}/M_Z^2)$ that give rise to large process-independent contributions which factorize from the LO cross section. Therefore, they are expected to result in a similar behaviour for both the on- and off-shell corrections. Comparing our results for the leading-jet $p_{\mathrm{T,jet}}$ in Figure 6 with Figure 5 in Ref. [30], we find agreement within 1−2% for $p_{\mathrm{T,jet}} > 200\,\mathrm{GeV}$. Only at smaller $p_{\mathrm{T,jet}}$, the details of the event definition start to be more relevant and the on-shell results deviate as expected. However, the good agreement between the two calculations is still remarkable, having in mind that in Ref. [30] both the QED corrections have been completely neglected and a different renormalization scheme ($\overline{\mathrm{MS}}$) has been adopted.

The contribution δ_γ from the photon-induced processes are small and only reach up to a few percent for large cut values where the EW and QCD corrections to the dominating tree processes are by far larger. Hence, we can safely neglect the corresponding NLO QCD corrections which are formally of the same order as the EW corrections to the partonic processes without a photon in the initial state.

The qualitative features of the corrections at the Tevatron are very similar to those at the LHC. Of course, at the Tevatron the high-energy (Sudakov) regime is not as accessible as at the LHC, but the onset of the Sudakov dominance is nevertheless visible as can be seen in Table 3 and Figure 6. We have adapted the range for the different integrated cross sections to the kinematic reach of the Tevatron.

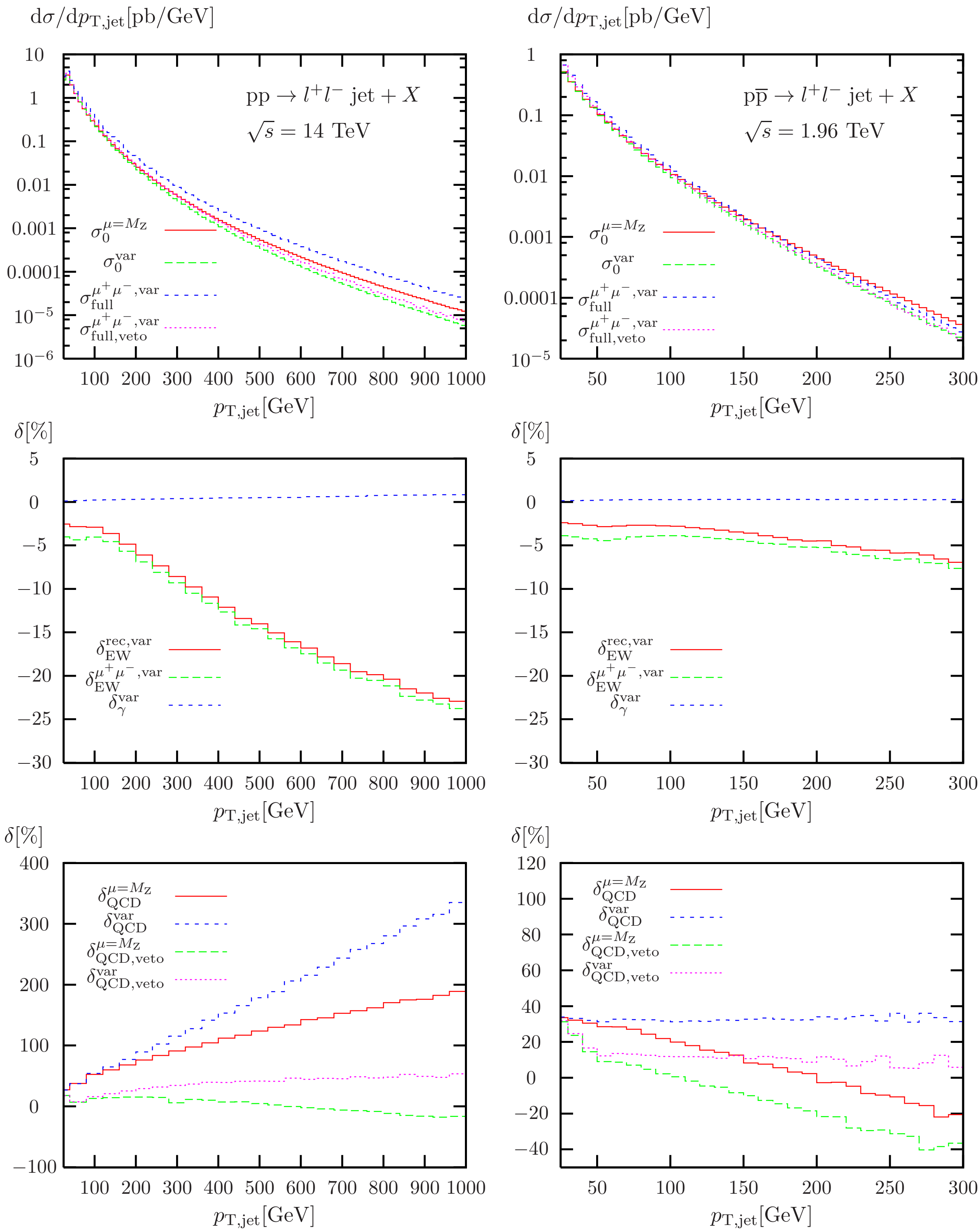

Figure 6: LO and fully corrected distribution (top), corresponding relative EW and photon-induced corrections (middle), and relative QCD corrections (bottom) for the transverse momentum of the leading jet at the LHC (left) and the Tevatron (right). See text for details.

$$\mathrm{pp} \to l^+l^- \,\mathrm{jet} + X \text{ at } \sqrt{s} = 14\,\mathrm{TeV}$$

$M_{ll}/\,\mathrm{GeV}$	$50-\infty$	$100-\infty$	$200-\infty$	$500-\infty$	$1000-\infty$	$2000-\infty$
$\sigma_0^{\mu=M_Z}/\,\mathrm{fb}$	123491(7)	7696.9(8)	628.47(6)	49.380(6)	5.1124(6)	0.27096(3)
$\sigma_0^{\mathrm{var}}/\,\mathrm{fb}$	122024(7)	7558.2(8)	602.45(5)	45.750(5)	4.5919(6)	0.23433(3)
$\delta_{\mathrm{EW}}^{\mu^+\mu^-,\mathrm{var}}/\%$	-4.2	$-9.3(1)$	-5.7	-9.5	$-15.1(1)$	$-23.8(1)$
$\delta_{\mathrm{EW}}^{\mathrm{rec},\mathrm{var}}/\%$	-2.8	-5.2	-3.0	-5.8	$-10.3(1)$	$-17.1(1)$
$\delta_{\mathrm{QCD}}^{\mu=M_Z}/\%$	35.8(1)	28.9(1)	12.0(1)	$-11.3(1)$	$-34.4(1)$	$-62.7(1)$
$\delta_{\mathrm{QCD}}^{\mathrm{var}}/\%$	35.9(1)	29.7(1)	14.7(1)	$-5.7(1)$	$-25.8(1)$	$-50.8(1)$
$\delta_{\mathrm{QCD,veto}}^{\mu=M_Z}/\%$	13.1(1)	6.8(1)	$-9.5(1)$	$-32.9(1)$	$-56.3(1)$	$-85.3(1)$
$\delta_{\mathrm{QCD,veto}}^{\mathrm{var}}/\%$	14.1(1)	8.7(1)	$-5.4(1)$	$-25.4(1)$	$-46.0(1)$	$-71.3(1)$
$\delta_{\gamma}^{\mathrm{var}}/\%$	0.1	0.9	2.7	2.9	2.6	2.3
$\sigma_{\mathrm{full,veto}}^{\mu^+\mu^-,\mathrm{var}}/\,\mathrm{fb}$	134266(49)	7580(9)	551.9(4)	31.10(5)	1.906(4)	0.0167(3)

Table 4: Integrated cross sections for different cuts on the dilepton invariant mass M_{ll} at the LHC with $\sqrt{s} = 14\,\mathrm{TeV}$. See caption of Table 1 and text for details.

Turning to the NLO QCD results at the LHC, we observe exactly the same qualitative results found for $\mathrm{W} + \mathrm{jet}$ production in Ref. [28]. As discussed above, the differential cross section for large $p_{\mathrm{T,jet}}$, as shown in Figure 6, contains large contributions from a completely different class of events for which two jets recoil against each other. Hence, the corrections are huge. The correction $\delta_{\mathrm{QCD}}^{\mu=M_Z}$ is smaller than $\delta_{\mathrm{QCD}}^{\mathrm{var}}$ because it is defined relative to a larger LO cross section. In absolute size, however, the NLO corrections are similar. Using the jet veto proposed at the end of Section 3.2.2, the corrections are reduced, and $\delta_{\mathrm{QCD}}^{\mathrm{var}}$ rises only to the 50% level for large cut values. The fixed scale choice accidentally leads to even smaller corrections $\delta_{\mathrm{QCD}}^{\mu=M_Z}$. As expected, the large discrepancy of the LO results for the two scale choices is largely removed by including the NLO corrections. However, varying the exact definition of the jet veto, the variable scale turns out to be more robust.

For the smaller CM energy $\sqrt{s} = 7\,\mathrm{TeV}$ the same qualitative behaviour is found (see Table 2 for the integrated results with varying cuts). At the Tevatron, the jet veto is not as important as at the LHC because of its kinematical limitations. On the other hand, as expected, the fixed scale choice leads to more and more negative corrections with increasing $p_{\mathrm{T,jet}}$, in particular when employing a jet veto. Using the variable scale stable results are obtained.

3.3.2 Dilepton invariant mass

Tables 4–6 show the analogous results for a variation of cuts on the dilepton invariant mass M_{ll}. The corresponding differential distributions for the Tevatron and the LHC at 14 TeV are displayed in Figure 7. Again, all other cuts and the corresponding event selection follow our default choice as introduced in Section 3.2.

In Tables 4–6, only the cross section in the first column includes resonant Z production. All the less inclusive cross sections only contain the tail of the distribution generated by (far) off-shell

$\mathrm{pp} \to l^+l^-\,\mathrm{jet} + X$ at $\sqrt{s} = 7\,\mathrm{TeV}$

$M_{ll}/\,\mathrm{GeV}$	$50-\infty$	$100-\infty$	$200-\infty$	$500-\infty$	$1000-\infty$	$2000-\infty$
$\sigma_0^{\mu=M_\mathrm{Z}}/\,\mathrm{fb}$	53029(3)	3259.1(4)	242.06(3)	13.300(2)	0.7276(1)	0.009264(9)
$\sigma_0^{\mathrm{var}}/\,\mathrm{fb}$	51949(3)	3171.4(4)	230.25(2)	12.283(2)	0.65366(9)	0.008059(8)
$\delta_{\mathrm{EW}}^{\mu^+\mu^-,\mathrm{var}}/\%$	-4.2	-9.3	-5.8	-10.2	$-16.7(1)$	$-27.7(1)$
$\delta_{\mathrm{EW}}^{\mathrm{rec},\mathrm{var}}/\%$	-2.7	-5.2	-3.0	-6.1	$-11.0(1)$	$-19.3(1)$
$\delta_{\mathrm{QCD}}^{\mu=M_\mathrm{Z}}/\%$	35.1(1)	28.3(1)	11.0(1)	$-11.8(1)$	$-34.0(1)$	$-63.5(7)$
$\delta_{\mathrm{QCD}}^{\mathrm{var}}/\%$	36.3(1)	30.4(1)	14.8(1)	$-5.3(1)$	$-25.0(1)$	$-50.4(2)$
$\delta_{\mathrm{QCD,veto}}^{\mu=M_\mathrm{Z}}/\%$	15.4(1)	9.3(1)	$-6.8(1)$	$-30.0(1)$	$-52.7(1)$	$-81.3(2)$
$\delta_{\mathrm{QCD,veto}}^{\mathrm{var}}/\%$	17.2(1)	12.0(1)	$-2.1(1)$	$-22.2(1)$	$-42.3(1)$	$-67.1(1)$
$\delta_{\gamma}^{\mathrm{var}}/\%$	0.2	1.0	2.9	3.0	2.8	3.0
$\sigma_{\mathrm{full,veto}}^{\mu^+\mu^-,\mathrm{var}}/\,\mathrm{fb}$	58823(23)	3290(4)	218.7(1)	8.67(1)	0.2861(6)	0.00065(1)

Table 5: Integrated cross sections for different cuts on the dilepton invariant mass M_{ll} at the LHC with $\sqrt{s} = 7\,\mathrm{TeV}$. See caption of Table 1 and text for details.

$\mathrm{p\bar{p}} \to l^+l^-\,\mathrm{jet} + X$ at $\sqrt{s} = 1.96\,\mathrm{TeV}$

$M_{ll}/\,\mathrm{GeV}$	$50-\infty$	$100-\infty$	$150-\infty$	$200-\infty$	$400-\infty$	$600-\infty$
$\sigma_0^{\mu=M_\mathrm{Z}}/\,\mathrm{fb}$	9648.3(3)	636.46(9)	121.20(1)	51.243(6)	3.9644(5)	0.41195(5)
$\sigma_0^{\mathrm{var}}/\,\mathrm{fb}$	9365.0(4)	614.55(9)	115.95(1)	48.770(5)	3.7177(4)	0.38255(5)
$\delta_{\mathrm{EW}}^{\mu^+\mu^-,\mathrm{var}}/\%$	-4.1	$-9.0(1)$	-5.8	-6.5	-11.1	$-15.7(1)$
$\delta_{\mathrm{EW}}^{\mathrm{rec},\mathrm{var}}/\%$	-2.6	-5.2	-3.1	-3.5	-6.6	$-9.5(1)$
$\delta_{\mathrm{QCD}}^{\mu=M_\mathrm{Z}}/\%$	30.7(1)	24.3(1)	15.3(1)	10.7(1)	$-0.3(1)$	$-8.0(2)$
$\delta_{\mathrm{QCD}}^{\mathrm{var}}/\%$	32.9(1)	26.7(2)	18.5(1)	14.7(1)	4.9(1)	$-2.0(1)$
$\delta_{\mathrm{QCD,veto}}^{\mu=M_\mathrm{Z}}/\%$	19.8(1)	13.8(2)	5.7(2)	1.1(1)	$-9.9(1)$	$-17.4(2)$
$\delta_{\mathrm{QCD,veto}}^{\mathrm{var}}/\%$	22.5(1)	16.7(2)	9.6(2)	5.7(1)	$-4.3(1)$	$-10.7(1)$
$\delta_{\gamma}^{\mathrm{var}}/\%$	0.2	0.7	1.2	1.0	0.5	0.3
$\sigma_{\mathrm{full,veto}}^{\mu^+\mu^-,\mathrm{var}}/\,\mathrm{fb}$	11102(6)	665(1)	121.7(2)	48.93(5)	3.162(2)	0.2825(4)

Table 6: Integrated cross sections for different cuts on the dilepton invariant mass M_{ll} at the Tevatron. See caption of Table 1 and text for details.

Z bosons and photons. Hence, the cross sections are smaller than for comparable cuts on $p_{\mathrm{T,jet}}$. Note that for a large cut on M_{ll} the cross section is dominated by events with a CM energy close to the M_{ll} cut since the leptons are mainly produced back to back and the additional jet is relatively soft. In comparison, for a large cut on $p_{\mathrm{T,jet}}$ the CM energy has to be more than twice the cut value because the transverse momentum of the jet has to be balanced.

The dilepton invariant-mass distribution is a crucial observable at the LHC, in particular for detector calibration and also in searches for heavy dilepton resonances. For calibration, the Z + jet channel is the main source for boosted Z bosons close to their mass shell resulting in high-energy leptons which are balanced by the hard jet. Hence, the precise theoretical understanding of the M_{ll} distribution, in particular around the Z-boson peak, is mandatory.

Concerning the EW corrections, the large Sudakov logarithms again result in large negative corrections at large values of the M_{ll} cut. They reach the level of -20% for $M_{ll} > 2000\,\mathrm{GeV}$. However, they cannot be compared to earlier on-shell computations since only off-shell Z bosons and photons contribute in the high-M_{ll} region as mentioned above.

As expected, the corrections for bare muons are larger since photons, being radiated collinearly to one of the charged leptons, carry away momentum and reduce the dilepton invariant mass if not recombined with the emitting lepton. This effect can be observed for any cut value in Tables 4–6. However, it is most prominent around the Z-boson peak in the differential distribution displayed in Figure 7. For bare muons, events that are enhanced by muon-mass logarithms are shifted to lower bins in the distributions. Hence, the correction is large and negative up to -20% around the Z peak. The correction below the Z resonance is positive. While the absolute correction compared to the differential cross section at the peak is relatively small, the relative correction to the distribution is huge because the LO result is relatively small away from the narrow Z-boson resonance. It amounts to more than 100% around a dilepton invariant mass of 75 GeV. The large correction, however, does not signal a breakdown of perturbation theory but only reflects the particular kinematic situation around the Z peak. If photons in a small cone around a radiating lepton are recombined, the corrections from almost collinear photons outside the cone are still sizeable and amount to roughly half the size of the corrections for bare muons. The size of the corrections is further reduced if the cone size for the lepton–photon recombination is increased. To reach an accuracy level of a few percent near the resonance, multi-photon radiation should be included in the calculation.

The CM energy at the LHC hardly plays any role for the size of the relative EW corrections. In Figure 8 we show the LO cross section and EW corrections for $\sqrt{s} = 7\,\mathrm{TeV}$. Only the LO cross section strongly depends on the CM energy. Even the results for the EW corrections at the Tevatron (see Figure 7) hardly differ from the ones at the LHC.

Since the dilepton mass is a property of the lepton–photon system only and it is invariant under boosts when recoiling against a hard QCD jet, our results can be compared to the EW corrections to the line shape of inclusive Z-boson production as, for instance, recently investigated in Ref. [13]. It turns out that the EW corrections are quite similar around the Z-boson peak. However, in the lower tail of the distributions the corrections only reach up to 80% in the inclusive analysis (see e.g. Figure 12 in Ref. [13]). A large part of this deviation can be attributed to the fact that the LO result for Z + jet production drops off faster than in the inclusive case, so that the relative corrections are different.

Turning again to NLO QCD, the corrections around the Z resonance in the invariant-mass distribution of the leptons are pretty flat since QCD can only indirectly affect the line shape of the colour-neutral Z boson. Depending on the exact event definition, the corrections amount to a few tens of percent. However, as shown in Table 4, in the high-invariant-mass tail both scale choices fail to reflect the kinematical situation, since the production of a far off-shell Z boson is

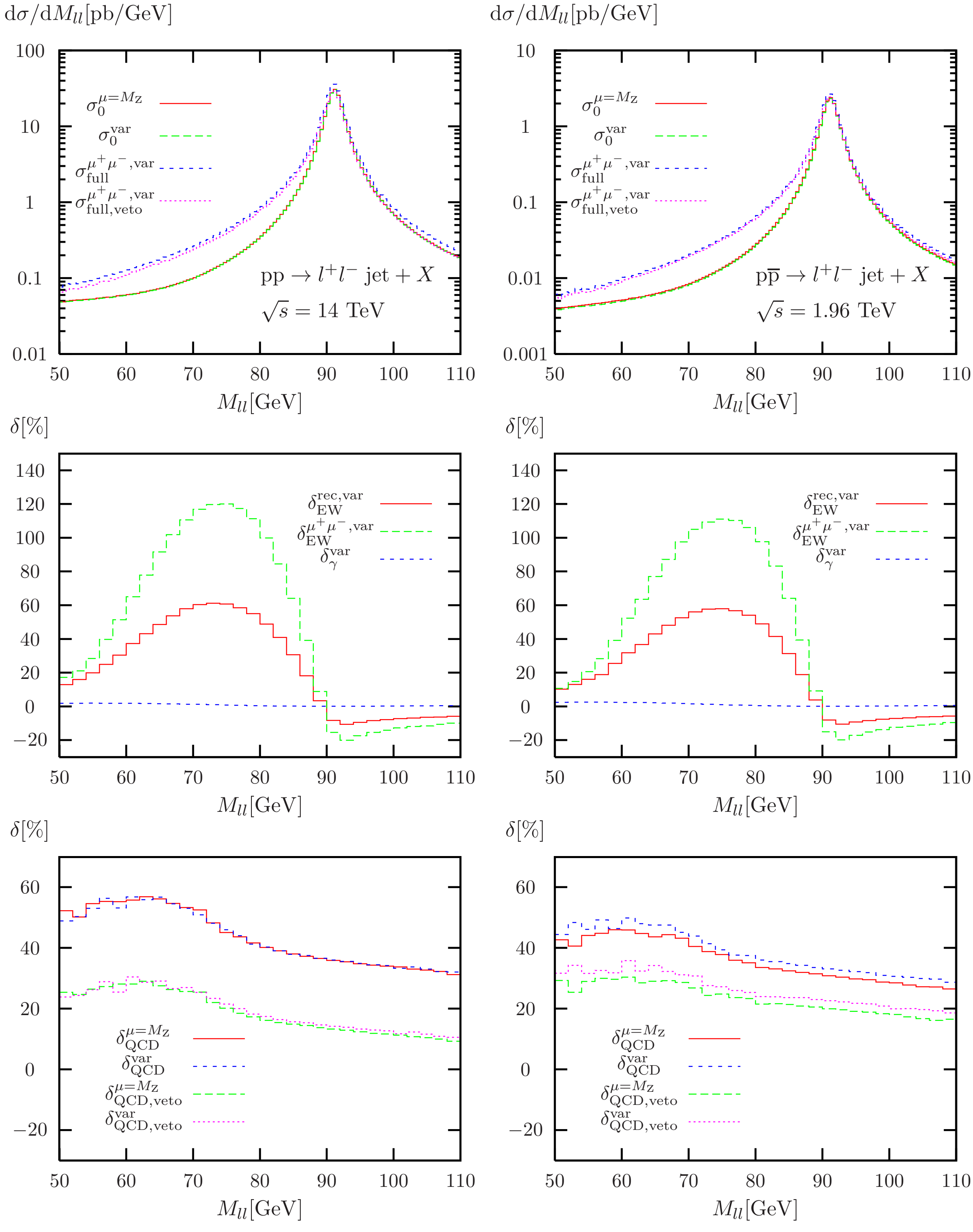

Figure 7: LO and fully corrected distribution (top), corresponding relative EW and photon-induced corrections (middle), and relative QCD corrections (bottom) for the dilepton mass at the LHC (left) and the Tevatron (right).

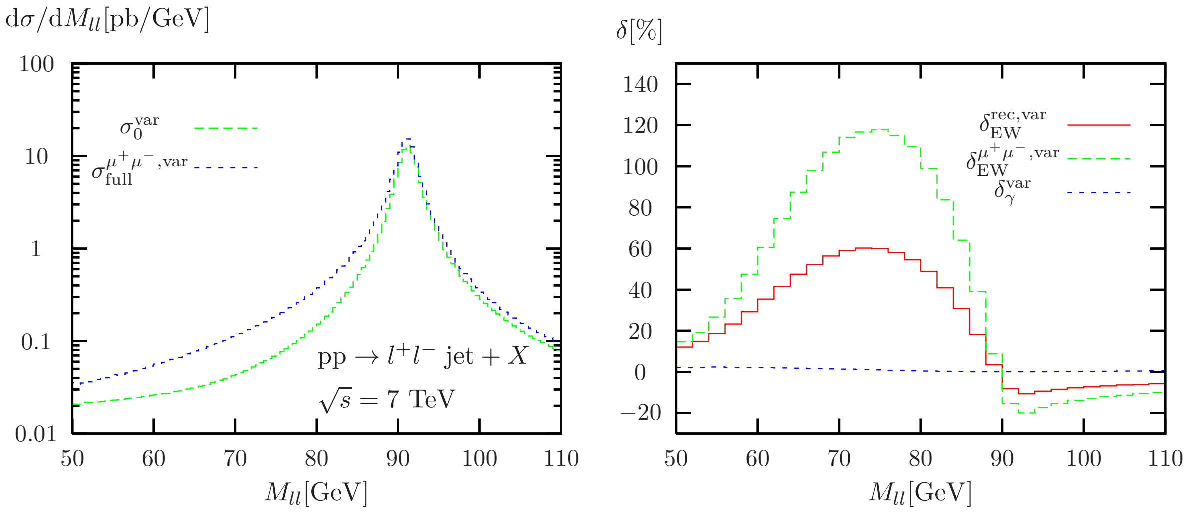

Figure 8: LO and fully corrected distribution (left) and corresponding relative EW and photon-induced corrections (right) for the dilepton mass at the LHC with $\sqrt{s} = 7\,\text{TeV}$.

dominated by the region near the threshold set by the cut on M_{ll}. In this region the Z boson decays mainly to back-to-back leptons with relatively soft jet activity. Hence, $\delta_{\rm QCD}^{\mu=M_Z}$ as well as $\delta_{\rm QCD}^{\rm var}$ become large and negative. A variable scale choice based on the CM energy of each event or a scale choice reflecting the invariant mass of the lepton pair would be more adequate. Since we focus on the EW corrections in this work we refrain from introducing yet another scale choice for the high-energy tail of this particular observable.

3.3.3 Transverse momentum of the charged leptons

In contrast to the invariant mass of the two charged leptons the transverse momentum of each of the leptons is sensitive to the recoil due to the hard jet in the event. Hence, the Jacobian peak of the transverse momentum at half the Z-boson mass in the inclusive Z-boson sample is washed out when an additional hard jet is present. The LO results and the corresponding correction for the positively charged lepton are shown in Figure 9. While the corrections are equivalent for the negatively charged lepton at the Tevatron, at the LHC they differ at the percent level but are qualitatively similar.

The EW corrections are at the percent level and quickly increase in size in the tail of the distribution for $p_{{\rm T},l^+} > 60\,\text{GeV}$, in particular for bare muons where they almost reach -10%. For even higher $p_{{\rm T},l^+} > 100\,\text{GeV}$ the typical increase of the correction due to the Sudakov logarithms can be observed. However, in contrast to the transverse-momentum distribution of the leading jet, the lepton–photon recombination still matters and the corrections differ by roughly 5% in the whole tail of the distribution.

The QCD corrections $\delta_{\rm QCD}$ for $p_{{\rm T},l^+}$ show pronounced dips where the LO cross section has peaks (see Figure 9). The real corrections do not particularly populate the regions of the distributions that are enhanced due to the particular LO kinematics. For $p_{{\rm T},l^+} < 100\,\text{GeV}$, $\delta_{\rm QCD}^{\mu=M_Z}$ and $\delta_{\rm QCD}^{\rm var}$ are practically identical. However, for larger transverse momenta, the corrections for the two scale choices differ significantly. Here, $\delta_{\rm QCD}^{\mu=M_Z}$ grows large and negative to compensate

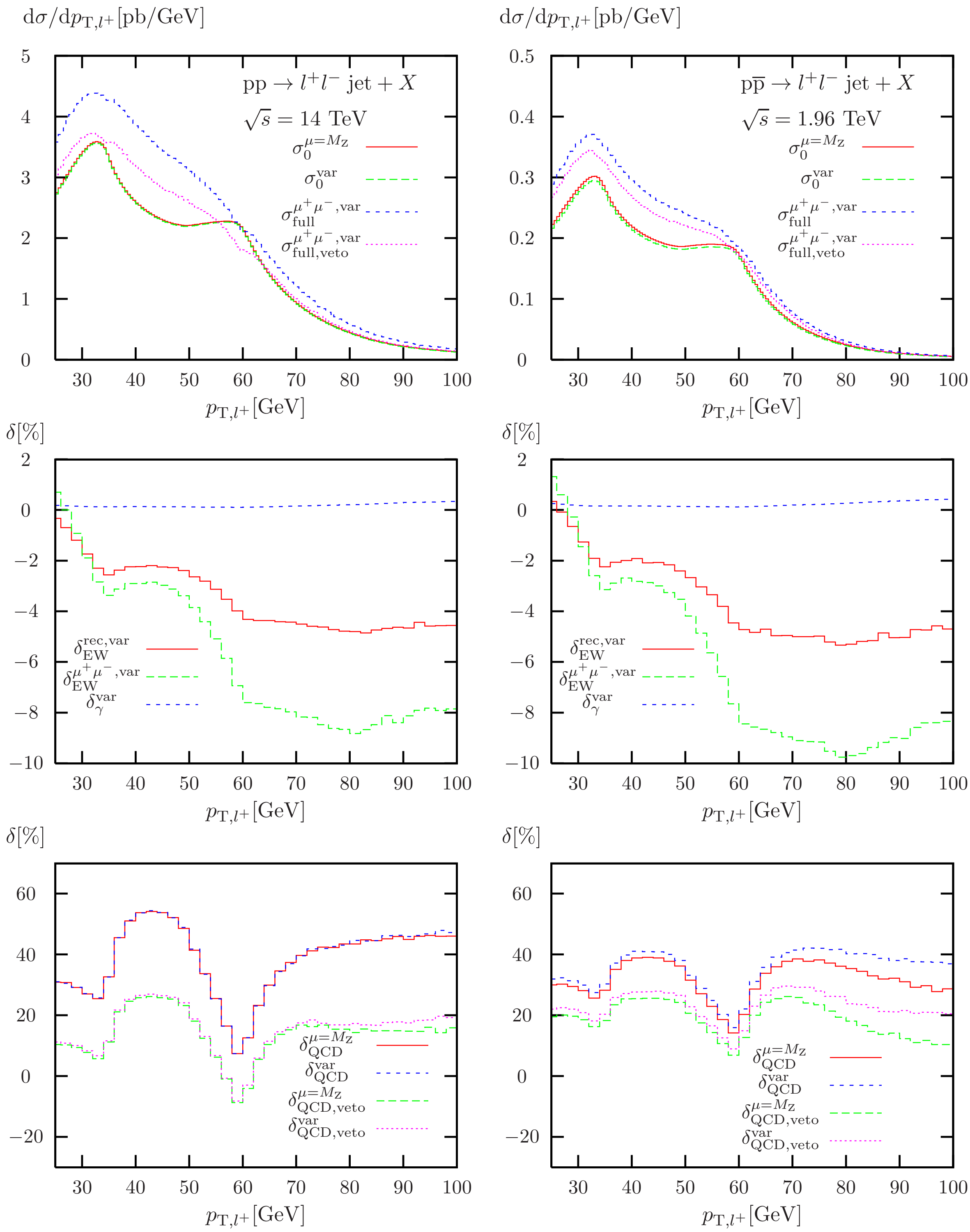

Figure 9: LO and fully corrected distribution (top), corresponding relative EW and photon-induced corrections (middle), and relative QCD corrections (bottom) for the transverse momentum of the positively charged lepton at the LHC (left) and the Tevatron (right).

for the overestimated LO cross section. This is expected, since the hard jet recoiling against the high-p_{T} lepton should be reflected in the scale choice.

At the Tevatron, the kinematical features are less pronounced and the deviation using a fixed scale starts already at $p_{\mathrm{T},l^+} \gtrsim 70\,\mathrm{GeV}$. However, all qualitative features for the EW as well as the QCD corrections are the same.

3.3.4 Transverse mass of the charged leptons

For Z-boson production, the transverse mass does not play a central role because the lepton system can be fully reconstructed. However, it is instructive to compare the transverse-mass distribution for Z + jet production with the corresponding distribution for W + jet. For W + jet, due to the neutrino in the final state, only the transverse mass but not the invariant mass of the two leptons can be measured. The distribution is displayed in Figure 10. It shows all the features of the analysis for W + jet discussed in detail in Ref. [28]. However, the EW corrections are roughly a factor of two larger and reach the level of -20% for bare muons in the interesting region around the Jacobian peak, simply because there are two charged leptons in the final state which radiate photons. This example indicates that one has to be especially careful when using ratios of W and Z cross sections with the aim to reduce theoretical and parametric (such as PDF) uncertainties. Even though the two systems are almost equivalent from the point of view of QCD, EW corrections differ significantly.

3.3.5 Rapidity distributions

In Figure 11, we display the results on the rapidity distribution for the positively charged lepton. For the LHC, the EW and QCD corrections are rather flat and only slightly increase the differential cross section in the forward and backward regions. The distribution and the corrections are symmetric with respect to $y_{l^+} = 0$. At the Tevatron, this symmetry is only slightly disturbed at LO and NLO QCD. However, the EW corrections are asymmetric, large and negative for $y_{l^+} = -2.5$, and almost zero for $y_{l^+} = 2.5$. Of course, the distribution for the rapidity of the negatively charged lepton shows the analogous behaviour with reversed rapidities w.r.t. the case of the l^+.

Concerning the rapidity of the leading jet y_{jet}, the EW corrections are flat and do not disturb the LO shapes of the distribution, as can be seen in Figure 12. The QCD corrections are only slightly larger in the forward and backward regions compared to the central region at the LHC.

Since both leptons can be fully reconstructed, also the rapidity y_{ll} of the final-state lepton pair—which resembles the rapidity of the intermediate boson—is experimentally accessible. The corresponding results are shown in Figure 13.

4 Conclusions

Following our study on W + jet production [28], we have presented the first calculation of the full EW NLO corrections to the production of two opposite-sign charged leptons in association with a hard jet at hadron colliders. For many observables the cross section is dominated by on-shell Z + jet production with a subsequent leptonic Z-boson decay. However, in our calculation all off-shell effects as well as the contributions of and the interference with an intermediate photon are taken into account, so that also observables that are not dominated by on-shell Z bosons are described with NLO accuracy in view of both QCD and EW corrections.

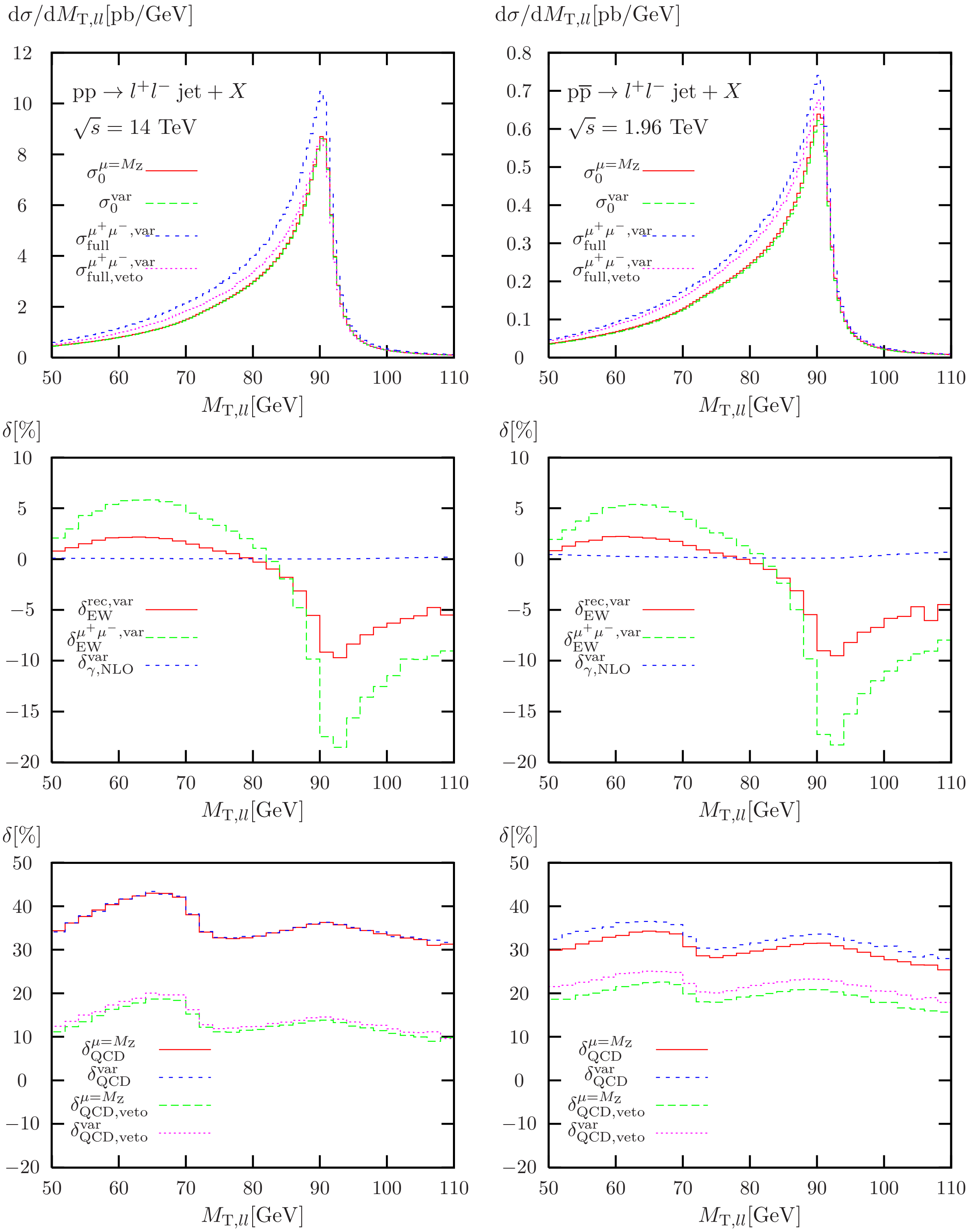

Figure 10: LO and fully corrected distribution (top), corresponding relative EW and photon-induced corrections (middle), and relative QCD corrections (bottom) for the transverse mass of the two charged leptons at the LHC (left) and the Tevatron (right).

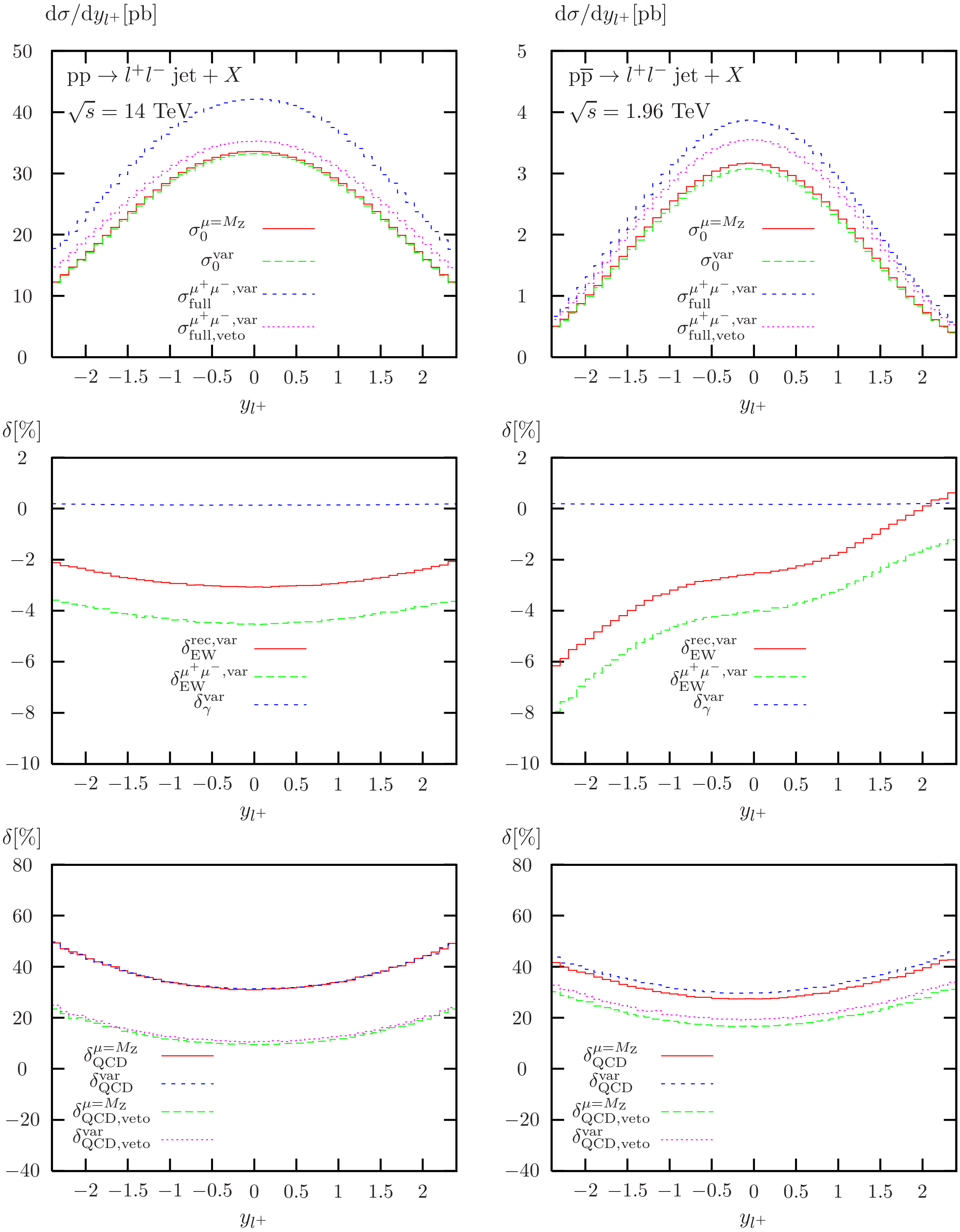

Figure 11: LO and fully corrected distribution (top), corresponding relative EW and photon-induced corrections (middle), and relative QCD corrections (bottom) for the rapidity of the positively charged lepton at the LHC (left) and the Tevatron (right).

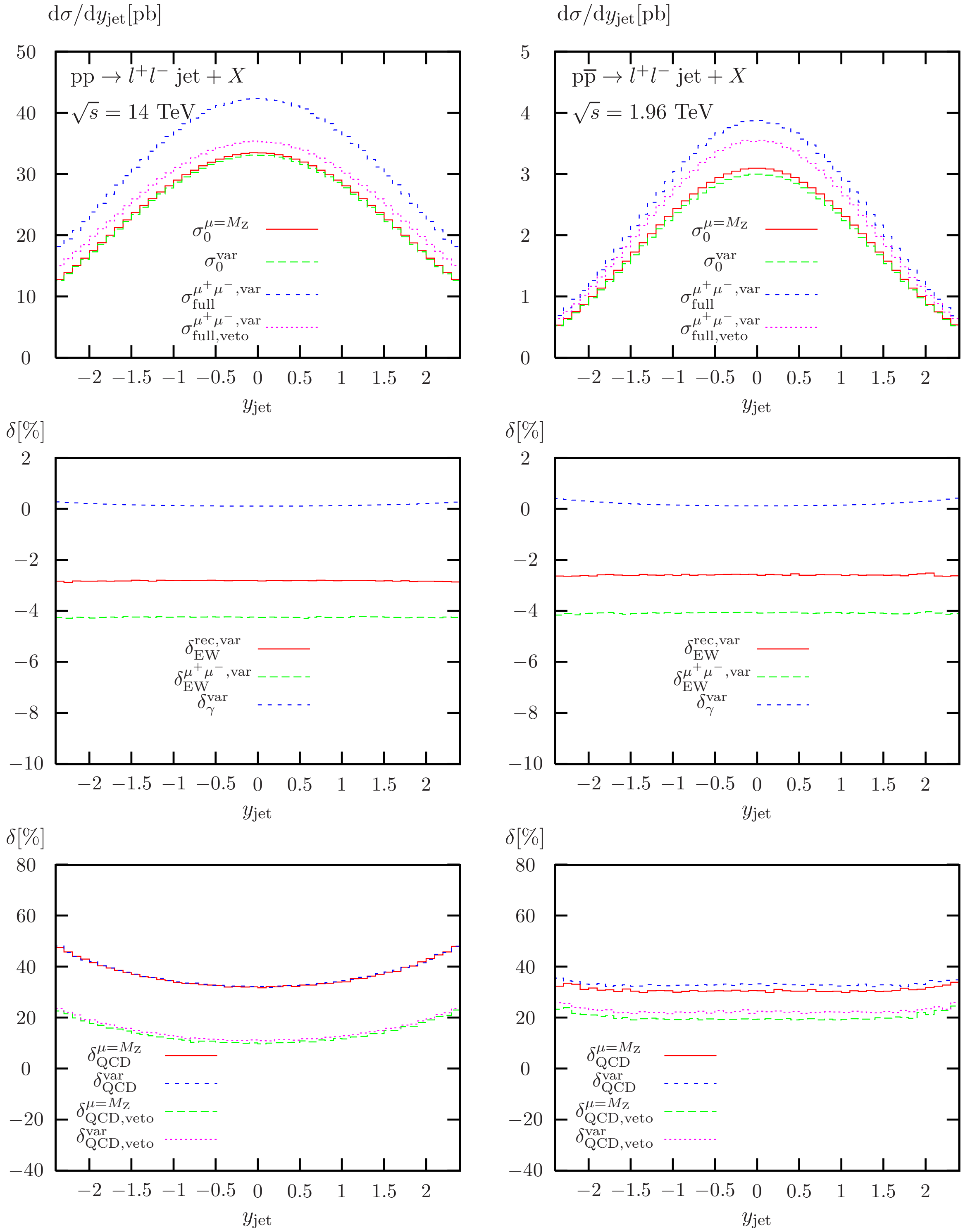

Figure 12: LO and fully corrected distribution (top), corresponding relative EW and photon-induced corrections (middle), and relative QCD corrections (bottom) for the rapidity of the leading jet at the LHC (left) and the Tevatron (right).

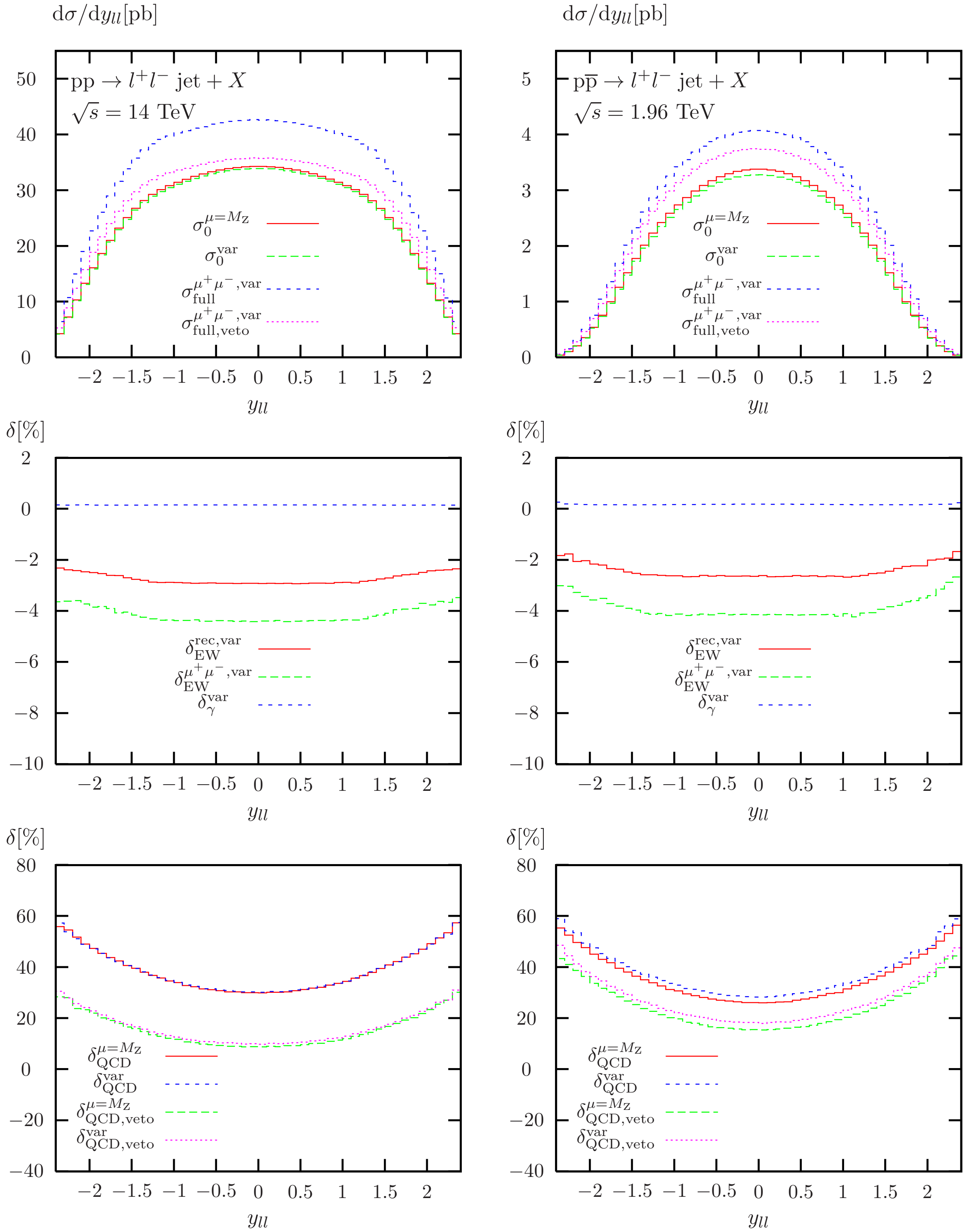

Figure 13: LO and fully corrected distribution (top), corresponding relative EW and photon-induced corrections (middle), and relative QCD corrections (bottom) for the rapidity of the dilepton system at the LHC (left) and the Tevatron (right).

We have implemented our results in a flexible Monte Carlo code which can model the experimental event definition at the NLO parton level. The distinction of $\mathrm{Z}+\mathrm{jet}$ and $\mathrm{Z}+\mathrm{photon}$ production is consistently implemented by making use of the measured quark-to-photon fragmentation function. We have also recalculated the NLO QCD corrections supporting a phase-space-dependent scale choice. Photon-induced processes are included at leading order but turn out to be phenomenologically unimportant.

The presented EW corrections are particularly large for the Z-boson line shape, i.e. the dilepton-invariant-mass distribution, mainly due to collinear final-state radiation. At the peak of the distribution, the corrections reach -20% for bare muons while they are at the order of 100% in the lower tail of the distribution, even larger than for the inclusive Z-boson line shape where no additional hard jet in the final state is demanded. When the EW corrections are not enhanced by final-state radiation due to particular kinematics, they are typically negative and at the level of a few percent. However, in the tail of distributions which are sensitive to large CM energies, the well-known Sudakov logarithms become dominant, and the EW corrections increase up to -25% at partonic $\sqrt{s} \sim 1\,\mathrm{TeV}$. For the p_{T} distribution of the jet, these results agree with earlier results in the on-shell approximation for the Z boson [30]. The QCD corrections have a typical size of a few tens of percent. However, they can become extremely large (hundreds of percent) at large jet p_{T} unless a sensible veto on a second hard jet is applied. The presented integrated cross sections and differential distributions demonstrate the applicability and flexibility of our setup which will be useful for accurate predictions of any observable in the investigated final state.

The importance of the neutral-current Drell–Yan process as a testing ground for perturbative calculations and for understanding and calibrating the detectors at the LHC can hardly be overestimated. Our calculation extends the availability of theoretical predictions for this process class to the EW corrections to associated production of Z bosons with a hard jet. Our calculation also constitutes one important part of a full NNLO prediction of the mixed EW and QCD corrections for inclusive Z production. In the range of intermediate and large transverse momenta of the additional hard jet our calculation delivers state-of-the-art predictions, for small transverse momenta the pure NLO calculation should of course be improved by dedicated QCD resummations, a task that goes beyond the scope of this paper.

Acknowledgements

This work is supported in part by the Gottfried Wilhelm Leibniz programme of the Deutsche Forschungsgemeinschaft (DFG), by the DFG Sonderforschungsbereich/Transregio 9 "Computergestützte Theoretische Teilchenphysik", and by the European Community's Marie-Curie Research Training Network HEPTOOLS under contract MRTN-CT-2006-035505.

References

[1] S. Haywood *et al.*, in *Standard Model Physics (And More) At The LHC*, eds. G. Altareli and M. Mangano (CERN-2000-004, Geneva, 2000), p. 117, hep-ph/0003275.

[2] C. E. Gerber *et al.* [TeV4LHC Top and Electroweak Working Group], "Tevatron-for-LHC report: Top and electroweak physics," arXiv:0705.3251 [hep-ph].

[3] R. Hamberg, W. L. van Neerven and T. Matsuura, Nucl. Phys. B **359** (1991) 343 [Erratum-ibid. B **644** (2002) 403];
W. L. van Neerven and E. B. Zijlstra, Nucl. Phys. B **382** (1992) 11 [Erratum-ibid. B **680** (2004) 513];

R. V. Harlander and W. B. Kilgore, Phys. Rev. Lett. **88** (2002) 201801 [hep-ph/0201206];
C. Anastasiou, L. J. Dixon, K. Melnikov and F. Petriello, Phys. Rev. Lett. **91** (2003) 182002 [hep-ph/0306192] and Phys. Rev. D **69** (2004) 094008 [hep-ph/0312266];
K. Melnikov and F. Petriello, Phys. Rev. Lett. **96** (2006) 231803 [hep-ph/0603182] and Phys. Rev. D **74** (2006) 114017 [hep-ph/0609070];
S. Catani, L. Cieri, G. Ferrera, D. de Florian and M. Grazzini, Phys. Rev. Lett. **103** (2009) 082001 [arXiv:0903.2120 [hep-ph]].

[4] S. Moch and A. Vogt, Phys. Lett. B **631** (2005) 48 [hep-ph/0508265];
E. Laenen and L. Magnea, Phys. Lett. B **632** (2006) 270 [hep-ph/0508284];
A. Idilbi, X. Ji, J. P. Ma and F. Yuan, Phys. Rev. D **73** (2006) 077501 [hep-ph/0509294];
V. Ravindran and J. Smith, Phys. Rev. D **76** (2007) 114004 [arXiv:0708.1689 [hep-ph]].

[5] S. Frixione and B. R. Webber, hep-ph/0612272;
S. Frixione, P. Nason and C. Oleari, JHEP **0711** (2007) 070 [arXiv:0709.2092 [hep-ph]];
S. Alioli, P. Nason, C. Oleari and E. Re, JHEP **0807** (2008) 060 [arXiv:0805.4802 [hep-ph]].

[6] P. B. Arnold and R. P. Kauffman, Nucl. Phys. B **349** (1991) 381;
C. Balazs, J. w. Qiu and C. P. Yuan, Phys. Lett. B **355** (1995) 548 [hep-ph/9505203];
C. Balazs and C. P. Yuan, Phys. Rev. D **56** (1997) 5558 [hep-ph/9704258];
R. K. Ellis, D. A. Ross and S. Veseli, Nucl. Phys. B **503** (1997) 309 [hep-ph/9704239];
R. K. Ellis and S. Veseli, Nucl. Phys. B **511** (1998) 649 [hep-ph/9706526];
J. w. Qiu and X. f. Zhang, Phys. Rev. Lett. **86** (2001) 2724 [hep-ph/0012058] and Phys. Rev. D **63** (2001) 114011 [hep-ph/0012348];
A. Kulesza and W. J. Stirling, Eur. Phys. J. C **20** (2001) 349 [hep-ph/0103089];
A. Kulesza, G. Sterman and W. Vogelsang, Phys. Rev. D **66** (2002) 014011 [hep-ph/0202251];
F. Landry, R. Brock, P. M. Nadolsky and C. P. Yuan, Phys. Rev. D **67** (2003) 073016 [hep-ph/0212159];
S. Berge, P. M. Nadolsky and F. I. Olness, Phys. Rev. D **73** (2006) 013002 [hep-ph/0509023];
G. Bozzi *et al.*, Nucl. Phys. B **815** (2009) 174 [arXiv:0812.2862 [hep-ph]].

[7] V. A. Zykunov, Eur. Phys. J. direct C **3** (2001) 9 [hep-ph/0107059].

[8] S. Dittmaier and M. Krämer, Phys. Rev. D **65** (2002) 073007 [hep-ph/0109062].

[9] U. Baur and D. Wackeroth, Phys. Rev. D **70** (2004) 073015 [hep-ph/0405191];
A. Arbuzov, D. Bardin, S. Bondarenko, P. Christova, L. Kalinovskaya, G. Nanava and R. Sadykov, Eur. Phys. J. C **46** (2006) 407 [Erratum-ibid. C **50** (2007) 505] [hep-ph/0506110].

[10] C. M. Carloni Calame, G. Montagna, O. Nicrosini and A. Vicini, JHEP **0612** (2006) 016 [hep-ph/0609170].

[11] U. Baur, S. Keller and W. K. Sakumoto, Phys. Rev. D **57** (1998) 199 [hep-ph/9707301];
U. Baur *et al.*, Phys. Rev. D **65** (2002) 033007 [hep-ph/0108274];
V. A. Zykunov, Phys. Rev. D **75** (2007) 073019 [hep-ph/0509315];
A. Arbuzov *et al.*, Eur. Phys. J. C **54** (2008) 451 [arXiv:0711.0625 [hep-ph]].

[12] C. M. Carloni Calame, G. Montagna, O. Nicrosini and A. Vicini, JHEP **0710** (2007) 109 [arXiv:0710.1722 [hep-ph]].

[13] S. Dittmaier and M. Huber, JHEP **1001** (2010) 060. [arXiv:0911.2329 [hep-ph]].

[14] C. M. Carloni Calame, G. Montagna, O. Nicrosini and M. Treccani, Phys. Rev. D **69** (2004) 037301 [hep-ph/0303102].

[15] W. Placzek and S. Jadach, Eur. Phys. J. C **29** (2003) 325 [hep-ph/0302065];
C. M. Carloni Calame, S. Jadach, G. Montagna, O. Nicrosini and W. Placzek, Acta Phys. Polon. B **35** (2004) 1643 [hep-ph/0402235].

[16] S. Brensing, S. Dittmaier, M. Krämer and A. Mück, Phys. Rev. D **77** (2008) 073006 [arXiv:0710.3309 [hep-ph]].

[17] S. Dittmaier and M. Krämer, in C. Buttar *et al.*, "Les Houches physics at TeV colliders 2005, standard model, QCD, EW, and Higgs working group: Summary report," hep-ph/0604120.

[18] A. B. Arbuzov and R. R. Sadykov, J. Exp. Theor. Phys. **106** (2008) 488 [arXiv:0707.0423 [hep-ph]].

[19] Q. H. Cao and C. P. Yuan, Phys. Rev. Lett. **93** (2004) 042001 [hep-ph/0401026];
B. F. L. Ward, C. Glosser, S. Jadach and S. A. Yost, Int. J. Mod. Phys. A **20** (2005) 3735 [hep-ph/0411047];
B. F. L. Ward and S. A. Yost, Acta Phys. Polon. B **38** (2007) 2395 [arXiv:0704.0294 [hep-ph]];
A. Vicini *et al.*, PoS **RADCOR2007** (2007) 013;
G. Balossini *et al.*, Nuovo Cim. **123B** (2008) 741;
A. Denner, S. Dittmaier, T. Kasprzik, and A. Mück, PoS **RADCOR2009**, 058 (2010) [arXiv:1001.2468 [hep-ph]].

[20] W. T. Giele, E. W. N. Glover and D. A. Kosower, Nucl. Phys. B **403** (1993) 633 [hep-ph/9302225].

[21] J. M. Campbell and R. K. Ellis, Phys. Rev. D **65** (2002) 113007 [hep-ph/0202176].

[22] J. J. van der Bij, E. W. N. Glover, Nucl. Phys. **B313** (1989) 237.

[23] C. F. Berger *et al.*, arXiv:1009.2338 [hep-ph];
C. F. Berger *et al.*, Phys. Rev. **D82** (2010) 074002. [arXiv:1004.1659 [hep-ph]];
C. F. Berger *et al.*, Phys. Rev. D **80** (2009) 074036 [arXiv:0907.1984 [hep-ph]];
R. K. Ellis, W. T. Giele, Z. Kunszt, K. Melnikov and G. Zanderighi, JHEP **0901**, 012 (2009) [arXiv:0810.2762 [hep-ph]].

[24] S. Alioli, P. Nason, C. Oleari, E. Re, JHEP **1101** (2011) 095. [arXiv:1009.5594 [hep-ph]].

[25] J. H. Kühn, A. Kulesza, S. Pozzorini and M. Schulze, Phys. Lett. B **651** (2007) 160 [hep-ph/0703283].

[26] J. H. Kühn, A. Kulesza, S. Pozzorini and M. Schulze, Nucl. Phys. B **797** (2008) 27 [arXiv:0708.0476 [hep-ph]].

[27] W. Hollik, T. Kasprzik and B. A. Kniehl, Nucl. Phys. B **790** (2008) 138 [arXiv:0707.2553 [hep-ph]].

[28] A. Denner, S. Dittmaier, T. Kasprzik, and A. Mück, JHEP **0908** (2009) 075. [arXiv:0906.1656 [hep-ph]].

[29] J. H. Kühn, A. Kulesza, S. Pozzorini and M. Schulze, Phys. Lett. **B609** (2005) 277-285. [hep-ph/0408308].

[30] J. H. Kühn, A. Kulesza, S. Pozzorini and M. Schulze, Nucl. Phys. **B727** (2005) 368-394. [hep-ph/0507178].

[31] P. Ciafaloni and D. Comelli, Phys. Lett. B **446** (1999) 278 [hep-ph/9809321];
V. S. Fadin, L. N. Lipatov, A. D. Martin and M. Melles, Phys. Rev. D **61** (2000) 094002 [hep-ph/9910338];
A. Denner and S. Pozzorini, Eur. Phys. J. C **18** (2001) 461 [hep-ph/0010201];
W. Beenakker and A. Werthenbach, Nucl. Phys. B **630** (2002) 3 [hep-ph/0112030];
A. Denner, M. Melles and S. Pozzorini, Nucl. Phys. B **662** (2003) 299 [hep-ph/0301241].

[32] A. Denner, S. Dittmaier, M. Roth and D. Wackeroth, Nucl. Phys. B **560** (1999) 33 [hep-ph/9904472].

[33] A. Denner, S. Dittmaier, M. Roth and L. H. Wieders, Nucl. Phys. B **724** (2005) 247 [hep-ph/0505042].

[34] D. Buskulic *et al.* [ALEPH Collaboration], Z. Phys. C **69** (1996) 365.

[35] A. D. Martin, R. G. Roberts, W. J. Stirling and R. S. Thorne, Eur. Phys. J. C **39** (2005) 155 [hep-ph/0411040].

[36] J. Küblbeck, M. Böhm and A. Denner, Comput. Phys. Commun. **60** (1990) 165;
H. Eck and J. Küblbeck, *Guide to FeynArts 1.0*, University of Würzburg, 1992.

[37] G. P. Lepage, J. Comput. Phys. **27** (1978) 192 and CLNS-80/447.

[38] T. Hahn, Comput. Phys. Commun. **140** (2001) 418 [hep-ph/0012260];
T. Hahn and C. Schappacher, Comput. Phys. Commun. **143** (2002) 54 [hep-ph/0105349].

[39] T. Hahn and M. Pérez-Victoria, Comput. Phys. Commun. **118** (1999) 153 [hep-ph/9807565].

[40] S. Dittmaier, Phys. Rev. D **59** (1999) 016007 [hep-ph/9805445].

[41] E. Accomando, A. Denner and C. Meier, Eur. Phys. J. C **47** (2006) 125 [hep-ph/0509234].

[42] S. Dittmaier and M. Roth, Nucl. Phys. B **642** (2002) 307 [hep-ph/0206070].

[43] J. Alwall *et al.*, JHEP **0709** (2007) 028. [arXiv:0706.2334 [hep-ph]].

[44] A. Denner and S. Dittmaier, Nucl. Phys. Proc. Suppl. **160** (2006) 22 [hep-ph/0605312].

[45] A. Denner, Fortsch. Phys. **41** (1993) 307-420. [arXiv:0709.1075 [hep-ph]].

[46] A. Denner and S. Dittmaier, Nucl. Phys. B **844** (2011) 199 [arXiv:1005.2076 [hep-ph]].

[47] G. 't Hooft and M. Veltman, Nucl. Phys. B **153** (1979) 365;
W. Beenakker and A. Denner, Nucl. Phys. B **338** (1990) 349;
A. Denner, U. Nierste and R. Scharf, Nucl. Phys. B **367** (1991) 637.

[48] S. Dittmaier, Nucl. Phys. B **675** (2003) 447 [hep-ph/0308246].

[49] D. B. Melrose, Nuovo Cim. **40** (1965) 181.

[50] A. Denner and S. Dittmaier, Nucl. Phys. B **658** (2003) 175 [hep-ph/0212259].

[51] A. Denner and S. Dittmaier, Nucl. Phys. B **734** (2006) 62 [hep-ph/0509141].

[52] G. Passarino and M. Veltman, Nucl. Phys. B **160** (1979) 151.

[53] A. Bredenstein, A. Denner, S. Dittmaier and S. Pozzorini, JHEP **0808** (2008) 108 [arXiv:0807.1248 [hep-ph]].

[54] S. Dittmaier, Nucl. Phys. B **565** (2000) 69 [hep-ph/9904440].

[55] S. Dittmaier, A. Kabelschacht and T. Kasprzik, Nucl. Phys. B **800** (2008) 146 [arXiv:0802.1405 [hep-ph]].

[56] T. Kinoshita, J. Math. Phys. **3** (1962) 650; T. D. Lee and M. Nauenberg, Phys. Rev. **133** (1964) B1549.

[57] A. Denner, S. Dittmaier, T. Gehrmann, C. Kurz, Nucl. Phys. **B836** (2010) 37 [arXiv:1003.0986 [hep-ph]].

[58] E. W. N. Glover and A. G. Morgan, Z. Phys. C **62** (1994) 311.

[59] S. Catani and M. H. Seymour, Nucl. Phys. B **485** (1997) 291 [Erratum-ibid. B **510** (1998) 503] [hep-ph/9605323].

[60] C. Amsler *et al.* [Particle Data Group], Phys. Lett. B **667** (2008) 1.

[61] D. Y. Bardin, A. Leike, T. Riemann and M. Sachwitz, Phys. Lett. B **206** (1988) 539.

[62] A. D. Martin *et al.*, Eur. Phys. J. **C63**, (2009) 189-285. [arXiv:0901.0002 [hep-ph]].

[63] M. R. Whalley, D. Bourilkov and R. C. Group, in *HERA and the LHC*, eds. A. de Roeck and H. Jung (CERN-2005-014, Geneva, 2005), p. 575, hep-ph/0508110.

[64] C. W. Bauer and B. O. Lange, arXiv:0905.4739 [hep-ph].

[65] G. C. Blazey *et al.*, in *QCD and Weak Boson Physics in Run II*, eds. U. Baur, R.K. Ellis and D. Zeppenfeld (Fermilab-Pub-00/297, Fermilab, 2000) p. 47, hep-ex/0005012.